




RESEARCH

Open Access



# Long term worsening of amyloid pathology, cerebral function, and cognition after a single inoculation of beta-amyloid seeds with Osaka mutation

Marina Célestine<sup>1,2</sup> , Muriel Jacquier-Sarlin<sup>3</sup>, Eve Borel<sup>3</sup>, Fanny Petit<sup>1,2</sup>, Jean-Baptiste Perot<sup>1,2</sup>, Anne-Sophie Hérard<sup>1,2</sup>, Luc Bousset<sup>1,2</sup>, Alain Buisson<sup>3</sup>  and Marc Dhenain<sup>1,2\*</sup> 

## Abstract

Alzheimer's disease (AD) is characterized by intracerebral deposition of abnormal proteinaceous assemblies made of amyloid- $\beta$  ( $A\beta$ ) peptides or tau proteins. These peptides and proteins induce synaptic dysfunctions that are strongly correlated with cognitive decline. Intracerebral infusion of well-defined  $A\beta$  seeds from non-mutated  $A\beta_{1-40}$  or  $A\beta_{1-42}$  peptides can increase  $A\beta$  depositions several months after the infusion. Familial forms of AD are associated with mutations in the amyloid precursor protein (APP) that induce the production of  $A\beta$  peptides with different structures. The  $A\beta$  Osaka ( $A\beta_{\text{Osa}}$  mutation (E693 $\Delta$ )) is located within the  $A\beta$  sequence and thus the  $A\beta_{\text{Osa}}$  peptides have different structures and properties as compared to non-mutated  $A\beta_{1-42}$  peptides ( $A\beta_{\text{wt}}$ ). Here, we wondered if a single exposure to this mutated  $A\beta$  can worsen AD pathology as well as downstream events including cognition, cerebral connectivity and synaptic health several months after the inoculation. To answer this question we inoculated  $A\beta_{1-42}$ -bearing Osaka mutation ( $A\beta_{\text{Osa}}$ ) in the dentate gyrus of APP<sub>SWE</sub>/PS1<sub>DE9</sub> mice at the age of two months. Their cognition and cerebral connectivity were analyzed at 4 months post-inoculation by behavioral evaluation and functional MRI.  $A\beta$  pathology as well as synaptic density were evaluated by histology. The impact of  $A\beta_{\text{Osa}}$  peptides on synaptic health was also measured on primary cortical neurons. Remarkably, the intracerebral administration of  $A\beta_{\text{Osa}}$  induced cognitive and synaptic impairments as well as a reduction of functional connectivity between different brain regions, 4 months post-inoculation. It increased  $A\beta$  plaque depositions and increased  $A\beta$  oligomers. This is the first study showing that a single, sporadic event as  $A\beta_{\text{Osa}}$  inoculation can worsen the fate of the pathology and clinical outcome several months after the event. It suggests that a single inoculation of  $A\beta$  regulates a large cascade of events for a long time.

**Keywords** Alzheimer's disease, Cerebral connectivity, Amyloid- $\beta$ ,  $A\beta$  Osaka, Memory, Synapses

\*Correspondence:

Marc Dhenain

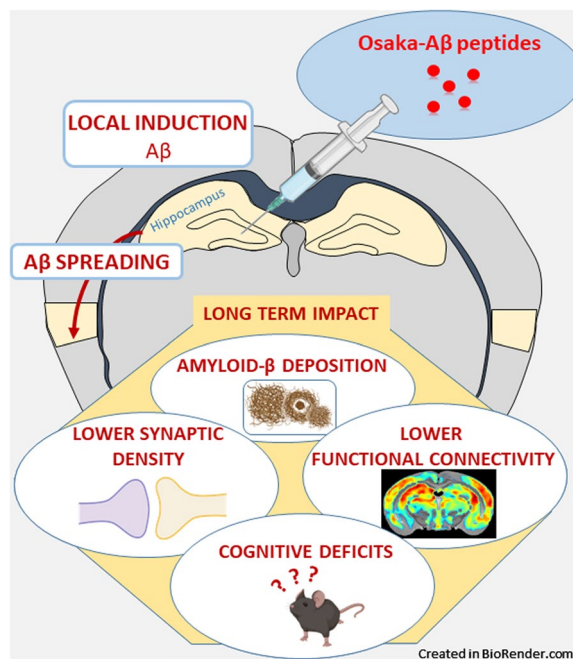
Marc.Dhenain@cnrs.fr

Full list of author information is available at the end of the article



© The Author(s) 2023. **Open Access** This article is licensed under a Creative Commons Attribution 4.0 International License, which permits use, sharing, adaptation, distribution and reproduction in any medium or format, as long as you give appropriate credit to the original author(s) and the source, provide a link to the Creative Commons licence, and indicate if changes were made. The images or other third party material in this article are included in the article's Creative Commons licence, unless indicated otherwise in a credit line to the material. If material is not included in the article's Creative Commons licence and your intended use is not permitted by statutory regulation or exceeds the permitted use, you will need to obtain permission directly from the copyright holder. To view a copy of this licence, visit <http://creativecommons.org/licenses/by/4.0/>. The Creative Commons Public Domain Dedication waiver (<http://creativecommons.org/publicdomain/zero/1.0/>) applies to the data made available in this article, unless otherwise stated in a credit line to the data.

## Graphical Abstract



## Introduction

Alzheimer's disease (AD) is a neurological disorder leading to cognitive deficits. It is characterized by intracerebral accumulation of abnormal proteinaceous assemblies made of amyloid- $\beta$  (A $\beta$ ) peptides or tau proteins. These peptides and proteins induce synaptic dysfunctions that are strongly correlated with the cognitive decline [20]. A $\beta$  peptides arise from the proteolytic cleavage of the A $\beta$  precursor protein (APP), leading to monomeric A $\beta$  peptides that can progressively aggregate to form fibrillary deposits (A $\beta$  plaques).

Several studies in humans [6, 14, 17] and in experimental animal models of AD [12, 19, 30, 31] indicate that intracerebral inoculation of minimal amounts of misfolded A $\beta$  present within AD brain extracts induces build-up of A $\beta$  deposits in their host. The intracerebral infusion of well-defined non-mutated A $\beta_{1-40}$  or A $\beta_{1-42}$  peptides can also increase A $\beta$  plaque depositions several months after the infusion [43, 49].

In addition to A $\beta$  pathology, the inoculation of AD-brain extracts can induce long-term cognitive alterations as well as synaptic impairments in rodents [24] or primates [12, 25]. As inoculation of AD-brain extracts can induce both A $\beta$  and tau pathologies [24], it is difficult to dissociate the role of A $\beta$  or tau on cognitive or synaptic impairments induced by this inoculation [24].

Thus, inoculation of synthetic or recombinant A $\beta$  seeds was proposed to evaluate the impact of A $\beta$  on brain function. However, although intracerebral infusion of these A $\beta$  seeds was shown to induce acute memory impairments in wild-type mice [2, 8], to our knowledge, their long term effects have not been reported on cognition or synaptic impairments.

Some familial forms of AD are associated with mutations in the A $\beta$  fragment of the APP. The Osaka mutation (E693 $\Delta$ , "Osa") is found in a Japanese pedigree of familial AD [46]. It corresponds to amino acid 693 deletion from APP gene, resulting in mutant A $\beta$  peptide (A $\beta_{\text{osa}}$ ) lacking a glutamic amino acid residue at the 22<sup>nd</sup> position. Thus, as the mutation is located within the A $\beta$  fragment, the A $\beta_{\text{osa}}$  peptides have a different structure and properties as compared to A $\beta_{\text{wt}}$  [37]. A $\beta_{\text{osa}}$  is more resistant than other A $\beta$  species to degradation by major A $\beta$ -degrading enzymes [46]. Synthetic A $\beta_{\text{osa}}$  have unique aggregation properties of enhanced oligomerization and no fibrillization [46]. This can be explained by the fact that they exhibit preferred conformational states that allow higher hydrophobicity resulting in faster oligomerization [15]. Consistent with the nonfibrillogenic property of the A $\beta_{\text{osa}}$ , a very low amyloid plaque load was observed in patient with this mutation [46] and transgenic mice with this mutation APP and they do not show any A $\beta$  plaques

even at 24 months but display an age-dependent accumulation of A $\beta$  oligomers within neurons [29, 45]. Given the different structure of A $\beta_{\text{osa}}$  peptides and their properties in vitro and in vivo, we wondered if exposure to A $\beta_{\text{osa}}$  can worsen AD pathology as well as downstream events including cognition, cerebral connectivity and synaptic health several months after the inoculation. The long-term effect of a single intra-hippocampal inoculation of A $\beta_{\text{osa}}$  seeds was evaluated four months post inoculation in transgenic mice (APP<sub>swe</sub>/PS1<sub>dE9</sub>) overexpressing A $\beta_{1-42}$  peptide and presenting A $\beta$  plaques [24]. Exposure to A $\beta_{\text{osa}}$  induced cognitive and functional impairments, including reduced hippocampal connectivity compared to mice inoculated with non-mutated A $\beta_{1-42}$  peptide (A $\beta_{\text{wt}}$ ). Exposure to A $\beta_{\text{osa}}$  also led to lower synaptic density and increased A $\beta$  plaque load and A $\beta$  oligomers. Our results suggest that the seeding induced by a single exposure to A $\beta_{\text{osa}}$  worsen the fate of A $\beta$  pathology and clinical outcome for several months.

## Methods

### Production of recombinant A $\beta$ proteins

To make the plasmids for the fusion protein A $\beta$ (His) of wild-type human  $\beta$ -amyloid 1–42 protein (A $\beta_{\text{wt}}$ ) or A $\beta_{\text{osa}}$  mutant (E22 $\Delta$ ), the cDNA containing the sequence for human A $\beta_{1-42}$  was obtained from synthetic oligonucleotides (Sigma, Lyon, France) (containing a NdeI restriction site as forward primers and a PspXI restriction site as reverse primers) using overlapping PCR. PCR products were then cloned into a pet28a-vector (Novagen, Paris, France) and subsequently constructed as various mutant HIS-A $\beta_{1-42}$  expressing plasmid (pet28a-A $\beta$ (His)<sub>wt</sub> or pet28a-A $\beta$ (His)<sub>osa</sub> (E22 $\Delta$ ). The resulting plasmids were verified by sequencing. *Escherichia Coli* BL21 (DE3) was transformed with the fusion protein plasmids and a single colony was chosen to grow in a 250 mL starter culture in Luria broth (LB medium) overnight at 37 °C. The next day, 10 mL of culture was diluted in 1L LB culture medium. When the culture reached an OD<sub>600nm</sub> of 0.8, isopropyl-beta-D-thiogalactopyranoside (IPTG) was added to 1 mM for induction. The culture was grown for an additional 4 h and the cells harvested by centrifugation at 4000 g for 20 min. The pellet was re-suspended in 10 mL ice-cold PBS and lysed by sonication at ice-cold temperature. The cell extract was then centrifuged at 20,000 g for 15 min at 4 °C. The pellet was re-suspended in 10 mL of 8 M urea in PBS and sonicated as previously described before centrifugation at 20,000 g for 15 min at 4 °C. The supernatant (5 mL) was diluted with 15 mL of binding buffer (PBS with 10 mM imidazole at pH 8.0). Before affinity purification using nickel-nitriloacetic acid (NTA) column purification, samples were filtered

on 0.45  $\mu$ m. The Ni-NTA column (3 mL of protino Ni-NTA Agarose from Macherey Nagel) was equilibrated with binding buffer prior to loading the sample on the column. Then the column was washed with the washing buffer (PBS with 30 mM imidazole at pH 8.0) with 5–10 column volumes. The protein was then eluted with the elution buffer (PBS with 500 mM imidazole at pH 7.4). The absorbance at 280 nm was used to monitor the elution but the concentration of the fusion proteins was estimated by comparing the intensity of the band of the protein on SDS-PAGE with that of a known quantity of BSA (Sigma, Lyon, France). A final concentration of 100  $\mu$ M was obtained and aliquots were stored at –80 °C. Aliquots from all subsequent purification steps were analyzed by SDS-PAGE [23], and the identity of A $\beta_{1-42}$  and mutants was verified by western blots using 4G8 monoclonal antibodies against A $\beta$  sequence (4G8).

### Endotoxin assay

Endotoxin content of A $\beta$  solutions was detected using a kinetic Limulus amoebocyte lysate (LAL) chromogenic endotoxin quantitation kit (Thermo Scientific). In brief, 50  $\mu$ M of A $\beta$  solution was prepared in PBS and was transferred to a sterile 96-well plate prewarmed to 37 °C. LAL (0.1 mL, room temperature) was quickly added to each well. Detection relied on standards supplied in the kit with the range from 0.10 to 1 EU/ml and on positive and negative controls that were performed at the same time as the samples. Endotoxin concentrations were determined by measuring kinetic absorbance at 405 nm at 37 °C following the instructions of the manufacturer, in a Spark plate reader (Tecan).

### Thioflavin T (ThT) binding assay

The aggregative properties of different forms of A $\beta$  can be evaluated in vitro with the well-characterized thioflavin dye binding assay [27]. First, the lyophilized synthetic A $\beta_{42}$  was purchased from Covalb (Villeurbanne, France). It was dissolved at a concentration of 1 mM in DMSO. A $\beta$  monomers stock solutions were generated by dilution of the peptides to a concentration of 100  $\mu$ M in phosphate buffer, pH 7.4.

Spontaneous fibril formation was evaluated by incubating 8  $\mu$ M of A $\beta$  monomer solutions at 37 °C for 24 h in presence of 10  $\mu$ M ThT (Wako Chemical Industries Ltd, Osaka, Japan) in phosphate buffer, pH 7.4. Fibril formation was followed by monitoring ThT fluorescence with shaking using a Hitachi F-2500 fluorometer. The excitation and emission wavelengths were 445 nm and 485 nm, respectively. Fluorescence was determined by averaging the three readings and subtracting the ThT blank.

To perform the seeding experiments, A $\beta_{\text{wt}}$  and A $\beta_{\text{osa}}$  solutions were rapidly thawed out and were added to the

synthetic  $A\beta_{1-42}$  + ThT solution previously described. All seeding experiments were performed with 10% or 2% of freshly prepared seeds and 90% or 98% of soluble  $A\beta$  monomers, resulting in a total of 8  $\mu\text{M}$ .  $A\beta_{\text{wt}}$  was used at 10% and  $A\beta_{\text{osa}}$  at 2 and 10%.

### Electron microscopy

$A\beta$  solutions (100  $\mu\text{l}$  sample of 8  $\mu\text{M}$ ) and fibrils obtained from 24 h ThT binding assay were concentrated tenfold by centrifugation at 50,000 g for 10 min and suspended in MilliQ water. Assemblies were layered on glow discharged carbon coated 400 mesh copper grid, and stained with 1% uranyl acetate. The assemblies were observed under Jeol 1400 electron microscope at 80 kV and 10 K magnification. Images were recorded on Rios CCD camera (Gatan).

### Primary cultures of cortical neurons

Mouse cortical neurons were cultured from 14- to 15-day-old OF1 embryos (Charles River) as described previously [26]. After extraction of the embryonic brains, the cerebral membranes were removed and the cortices were dissected, mechanically dissociated and cultured in Dulbecco's Modified Eagle's Medium supplemented with 5% horse serum, 5% fetal bovine serum and 1 mM glutamine (all from Sigma) on 24-well plates (Falcon; Becton Dickinson) for biochemical experiments.

Neurons were seeded on 35 mm glass-bottom dishes (MatTek) at a final concentration of two cortical hemispheres per dish for confocal experiments. All plates, dishes, and coverslips were coated with 0.1 mg/mL poly-D-lysine and 0.02 mg/mL laminin (Sigma). Cultures were maintained at 37 °C in a humidified atmosphere containing 5% CO<sub>2</sub>/95% air. After 3–4 days in vitro (DIV), cytosine arabinoside (AraC, 10  $\mu\text{M}$ ; Sigma) was added to inhibit proliferation of non-neuronal cells in cultures used for biochemistry experiments; 98% of the cells were considered as neuronal. The day before the experiments, cells were washed in DMEM. Treatments were performed on neuronal cultures at 14–15 DIV.

### Quantification and morphological characterisation of dendritic spine density

Neurons were visualized using a Nikon Ti C2 confocal microscope with a Nikon 60X water-immersion objective and NIS-Elements software (Nikon, Melville, NY, USA). Excitation of GFP and mCherry fluorophores was performed with an argon laser at 488 nm (emission filtered at 504–541 nm) and at 543 nm (emission filtered at 585–610 nm) respectively. Images (1024 × 1024 pixels) were acquired as Z-stacks (tridimensional section) with 0.3  $\mu\text{m}$  per step. The acquired images were then

deconvoluted using AutoQuantX3 software (Media Cybernetics, Abingdon, Oxon, UK). For analysis of spines, serial image files corresponding to z-stacks of 20–30 optical sections per dendritic segment were directly processed with NeuronStudio, a software package specifically designed for spine detection and analysis (<https://biii.eu/neuronstudio>, CNIC – Mount Sinai School of Medicine). Voxel size was 0.3 × 0.3 × 0.3  $\mu\text{m}$ . After modeling of the dendrite surface, protrusions with a minimum volume of 5 voxels, length of between 0.2  $\mu\text{m}$  and 4  $\mu\text{m}$  and a maximal width of 3  $\mu\text{m}$  were retained as spines. Following default settings of the program and the empirical classification rule previously described [35], spines with a minimum head diameter of 0.35  $\mu\text{m}$  and minimum head vs neck ratio of 1.1 were classified as mushroom spines. Non-mushroom spines with minimum volume of 10 voxels (0.040  $\mu\text{m}^3$ ) were classified as stubby spines. All other spines were considered thin.

### Transgenic mice

Mouse experiments involved the  $APP_{\text{swe}}/PS1_{\text{dE9}}$  mouse model of amyloidosis (C57Bl6 background) [11].  $A\beta$  plaques can be detected as early as 4 months of age in these mice and increase in number and total area with age [11]. At the time of the inoculation of  $A\beta_{\text{wt}}$ ,  $A\beta_{\text{osa}}$  or PBS, at 2 months of age, these mice did not have  $A\beta$  plaques. Animals were studied for four months after intracerebral inoculation (at 4 post-inoculation (mpi) respectively,  $n_{APP/PS1-A\beta_{\text{wt}}}=10$ ,  $n_{APP/PS1-A\beta_{\text{osa}}}=10$ ,  $n_{APP/PS1-PBS}=10$ ). Wild-type littermates injected with the PBS were used as controls for the behavioral tests ( $n_{WT-PBS}=10$ ). All  $APP_{\text{swe}}/PS1_{\text{dE9}}$  and littermate WT mice were born and bred in our center (Commissariat à l'Energie Atomique, Fontenay-aux-Roses; European Institutions Agreement #B92-032-02). Females were exclusively used in this study in order to optimize group homogeneity ( $A\beta$  plaque load is known to vary between males and females). Mice were injected during different inoculation sessions and each group was randomly inoculated at each session to avoid an "order of treatment" confounding effect. All animals were randomly assigned to the experimental groups using a simple procedure: They were identified using increasing numbers based on their birthdate. Animals with increasing numbers were alternatively assigned to the  $APP/PS1-A\beta_{\text{wt}}$  (animal 1, 4, 7...),  $APP/PS1-A\beta_{\text{osa}}$  (animal 2, 5, 8...) and  $APP/PS1-PBS$  groups (animal 3, 6, 9...). All experimental procedures were conducted in accordance with the European Community Council Directive 2010/63/UE and approved by local ethics committees (CEtEA-CEA DSV IdF N°44, France) and the French Ministry of Education and Research, and in compliance

with the 3R guidelines. Animal care was supervised by a dedicated in-house veterinarian and animal technicians. Human endpoints concerning untreatable continuous suffering signs and prostrations were taken into account and not reached during the study. Animals were housed under standard environmental conditions (12-h light–dark cycle, temperature:  $22 \pm 1$  °C and humidity: 50%) with ad libitum access to food and water. The design and reporting of animal experiments were based on the ARRIVE reporting guidelines [5]. Sample size was based on previous experiments for A $\beta$  induction in APP<sub>swe</sub>/PS1<sub>dE9</sub> mice after inoculation of human brain extracts (estimated with significance level of 5%, a power of 80%, and a two-sided test) [12] and increased to take into account uncertainties for new markers (memory and synaptic changes). No animals were excluded from the study. MC was aware of initial group allocation, but further analyses (memory evaluations and post-mortem studies) were performed blindly.

### Stereotaxic surgery

Five-hundred micrograms/ml (~150 nM) of A $\beta$ <sub>wt</sub>, A $\beta$ <sub>osa</sub> solution were rapidly thawed out before stereotaxic injection. Two month-old APP<sub>swe</sub>/PS1<sub>dE9</sub> and wild-type littermates were anesthetized by an intraperitoneal injection of ketamine (1 mg/10 g; Imalgène 1000, Merial) and xylazine (0.1 mg/10 g; 2% Rompun, Bayer Healthcare). Local anesthesia was also performed by a subcutaneous injection of lidocaine at the incision site (1  $\mu$ L/g; 0.5% Xylovet, Ceva). Mice were placed in the stereotaxic frame (Phymep) and bilateral injections of brain samples were performed in the dentate gyrus (AP -2 mm, DV 1.8 mm,  $L \pm 2$  mm from bregma). Two  $\mu$ l/site of sample were administered using 34-gauge needles and Hamilton syringes, at a rate of 0.2  $\mu$ l/min. After the injection, needles were kept in place for 5 more minutes before removal and the incision was sutured. The surgical area was cleaned before and after the procedure using povidone iodine (Vétédine, Vétquinol). Respiration rate was monitored and body temperature was maintained at  $37 \pm 0.5$  °C with a heating pad during the surgery. Anesthesia was reversed with a subcutaneous injection of atipamezole (0.25 mg/kg; Antisedan, Vetoquinol). Mice were placed in a ventilated heating box (25 °C) and monitored until full recovery from anesthesia. Postoperative anticipatory pain management consisted of paracetamol administration in drinking water (1.45 mL/20 mL of water; Doliprane, Sanofi) during 48 h.

### Behavioral evaluations

A novel object recognition task in a V-maze was used to investigate cognition at 4 mpi on A $\beta$ <sub>wt</sub>, A $\beta$ <sub>osa</sub>, and PBS-inoculated APP<sub>swe</sub>/PS1<sub>dE9</sub> mice. Wild-type littermates

injected with PBS were used as controls for the tests. Mice were handled for 2 min per day, for 5 days prior to any test to prevent stress effects during tasks. Prior to each test, mice were habituated to the experimental room for 30 min. The experimenter was blind to mouse groups. Performances were recorded using a tracking software (EthoVision XT14, Noldus).

The V-maze arena consisted of two 6 cm-wide, 33.5 cm-long and 15 cm-high black arms forming a V shape and exposed to 50 lx-lighting. The test was divided into three phases, each one separated by 24 h. At the beginning of each session, mice were placed at the center of the arena, *i.e.* at the intersection of the arms. During the habituation phase (day 1), mice were free to explore the empty arena for 9 min. The distance traveled was automatically recorded as an indicator of their exploratory activity. For the training phase (day 2), two identical objects (bicolor plastic balls) were placed at the end of each arm. Exploratory activity was evaluated as the time spent exploring the objects (manually recorded) and the distance traveled during the 9-min trial. On the test day (day 3), one familiar object (a bicolor plastic ball) was replaced by a novel one of a different shape and material (a transparent glass flask). Recognition was assessed using a discrimination index, calculated as follows:

Discrimination index

$$= \frac{\text{Time exploring the novel object} - \text{Time exploring the familiar object}}{\text{Total exploration time}}$$

It reflects the time spent exploring each object, and therefore, the ability to discriminate a novel object from a familiar, previously explored one. A low discrimination index score reveals that mice spent less time exploring the new object, *i.e.* still had marked interest in the familiar object, and suggests that memory was impaired. Between each run, the V-maze was cleaned with 10% ethanol, effectively eliminating any scents from previous visits.

### Animal preparation and MRI acquisition

To further evaluate brain function, we performed resting-state functional magnetic resonance imaging studies (fMRI) at 4 mpi. Our objective was i. to analyze the strength of the hippocampus functional connectivity (FC) to the whole-brain, ii. to analyze the FC of specific regions of the hippocampus and of the entorhinal cortex to the whole-brain. Animals were scanned four months post-inoculations. Acquisitions were performed on anesthetized mice with a combination of isoflurane 0.5% in a mix 0.5:0.5 of air:O<sub>2</sub> and medetomidine 0.3 mg/kg bolus and 0.1 mg/kg/h infusion. Animals were freely-breathing and respiratory rate was monitored to confirm animal

stability until the end of the experiment. Body temperature was maintained by a water heating system at 37 °C. The MRI system was an 11.7 Tesla Bruker BioSpec (Bruker, Ettlingen, Germany) using a Cryoprobe surface and running ParaVision 6.0.1. First, anatomical images were acquired using a T2-weighted multi-slice multi-echo (MSME) sequence: TR=1000 ms, TE=5 ms, 6 echoes, inter-echo time=5 ms, FOV=16 × 16 mm, 100 slices of 0.2 mm thickness, resolution=200 μm isotropic, acquisition duration 10 min. Then, resting-state functional MRI (rs-fMRI) was acquired using a gradient-echo echo planar imaging (EPI) sequences with repetition time (TR)=1000 ms, echo time (TE)=10 ms, flip angle=90°, volumes=500, Field of view (FOV)=22.5 × 15.4 mm, 12 slices of 0.5 mm thickness, acquisition duration 7 min 30 s. Animals were scanned twice with this sequence. For analysis, the two scans were merged.

### MRI pre-processing and analysis

Scanner data were exported as DICOM files then converted into NIFTI-1 format. Then spatial pre-processing was performed using the python module *sammba-mri* (SmAll MaMmals BrAin MRI; <http://sammba-mri.github.io>, [3]). First, spatial normalization of the anatomical images was performed to generate a high-resolution template. Rs-fMRI images were corrected for slice timing (interleaved), motion, and B0 distortion (per-slice registration to respective anatomicals). Then, rs-fMRI images were co-registered to the high-resolution template of the DSURQE anatomical atlas (Dorr-Steadman-Ulman-Richards-Qiu-Egan (DSURQE) atlas, 182 structures, freely available at: <https://wiki.mouseimaging.ca/display/MICePub/Mouse+Brain+Atlases>) [4, 34, 42, 48]. Functional images were further pretreated using Nilearn [1]. Nuisance signal regression was applied including a linear trend as well as 24-motion confounds (6 motion parameters, those of the preceding volume, plus each of their squares [10]). Images were then spatially smoothed with a 0.4 mm full-width at half-maximum Gaussian filter. The first 10 volumes were excluded from analysis after the preprocessing to ensure steady-state magnetization.

### MRI analysis and statistics

We analyzed the strength of the hippocampus functional connectivity (FC) to the whole-brain. First, we quantified the whole-brain pattern of functional connectivity for each subject by computing Pearson's correlation coefficients between mean time series of 70 bilateral regions defined from a brain atlas. The average correlation coefficient between the hippocampus and all other brain areas was then evaluated. Second, we evaluated FC of three selected brain regions (right hemisphere) to the whole-brain: the MoDG (inoculation site), the CA1 area

(which contains the pyramidal cell layer (CAPy)) and the entorhinal cortex. We used a “seed-based analysis” (SBA) to identify regions functionally associated with each selected brain region. This method assesses the connection between cluster of voxels (called seeds) positioned in the brain. Here the seeds (in MoDG, CAPy or entorhinal cortex) were defined based on the DSURQE Dorr atlas using 0.3 mm<sup>3</sup> spheres, corresponding to 25 voxels. The mean BOLD signal time-series within a seed were extracted and regressed into individual scans to obtain correlation z-statistic maps using Nilearn. Voxelwise statistics were carried out in FSL using nonparametric permutation tests (randomize) for comparison between PBS- inoculated APP<sub>swe</sub>/PS1<sub>dE9</sub> and either Aβ<sub>wt</sub>- or Aβ<sub>osa</sub>-inoculated APP<sub>swe</sub>/PS1<sub>dE9</sub> (5000 permutations and voxelwise correction). 3D representation of voxelwise statistical maps are shown as color-coded t-statistics overlays on the DSURQE template at 0.04 × 0.04 × 0.04 mm<sup>3</sup> using MRICroGL (<https://www.nitrc.org/projects/mricrogl/>).

### Animal euthanasia and brain preparation

Mice were sacrificed at 4 mpi, after MRI acquisition, with an intraperitoneal injection of a lethal dose of pentobarbital (100 mg/kg; Exagon, Axience). They were perfused intracardially with cold sterile 0.1 M PBS for 4 min, at a rate of 8 ml/min. The brain was extracted and separated in two hemispheres. The left hemisphere was dissected in order to take out the hippocampus and the cortex. Samples were directly deep-frozen into liquid nitrogen and stored at −80 °C for biochemical analysis. For histology, the right hemisphere was post-fixed in 4% paraformaldehyde for 48 h at +4 °C, transferred into a 15% sucrose solution for 24 h and in a 30% sucrose solution for 48 h at +4 °C for cryoprotection. Serial coronal sections of 40 μm were performed with a microtome (SM2400, Leica Microsystems) and stored at −2 °C in a storing solution (glycerol 30%, ethylene glycol 30%, distilled water 30%, phosphate buffer 10%).

### Mouse brain sample preparation for biochemical analyses

For amyloid protein extraction, deep-frozen brain tissue was dissociated with Collagenase D (2 mg/mL) in Tris-buffer saline (20 mM Tris-HCl, 150 mM NaCl, pH 7.4) at 1:10 TBS volume:brain wet weight and incubated at 37 °C. Brains were further homogenized using a Dounce homogenizer with 20 strokes in ice-cold quench buffer containing protease inhibitors (Complete, PMSF 1 mM) and phosphatase inhibitors (Na<sub>3</sub>VO<sub>4</sub> 1 mM, NaF 10 mM). Sarkosyl (2%) were added to homogenates. Samples were centrifuged for 30 min at 10,000 × g at 4 °C. The resulting supernatant was further centrifuged for 1 h at 100,000 g in a 4 °C TLA100.2 rotor on Beckman TL

100. The resulting supernatant called S100K contained the sarkosyl-soluble fraction. Pellet (P100K) was washed twice in TBS and finally resuspended in TBS at 1:10 TBS volume:brain wet weight. All samples were stored at  $-80^{\circ}\text{C}$  until analysis.

#### Western blotting and dot blotting

For western blot, samples were diluted in LDS (Lithium Dodecyl Sulfate) sample buffer (NuPage) and sampling reducing agent in order to load  $20\ \mu\text{g}$  of proteins. After heating, samples were loaded on a 4–12% Criterion<sup>TM</sup> XT Bis–Tris gel (Bio-Rad), migrated in XT MES Running Buffer (Bio-Rad) for 1 h at 110 V and transferred onto  $0.2\ \mu\text{m}$  nitrocellulose. For dot blot,  $2\ \mu\text{L}$  of samples were directly loaded onto  $0.2\ \mu\text{m}$  nitrocellulose. After 1 h of blocking at room temperature, membranes were blotted overnight at  $4^{\circ}\text{C}$  with primary antibodies 6E10 (Against human  $\text{A}\beta_{1-16}$ ; Biolegend), APP-Cter-17 (against the last 17 amino acids of the human APP sequence [39, 51], A11 (against oligomeric species, ThermoFisher) and OC (anti-amyloid fibrils, Rockland). After rinse in TBS-T, membranes were incubated with secondary antibodies for 1 h at room temperature. Proteins were revealed using horseradish peroxidase (HRP) and ECL<sup>TM</sup> Western Blotting Detection Reagent (G&E Healthcare). Quantifications of protein expression levels were performed on ImageJ Software.

#### Immunohistochemistry

$\text{A}\beta$  deposits were evaluated using a 4G8 labeling. Free-floating brain sections were rinsed in a 0.1 M PBS solution (10% Sigma-Aldrich<sup>®</sup> phosphate buffer, 0.9% Sigma-Aldrich<sup>®</sup> NaCl, distilled water) before use. Washing and incubation steps were performed on a shaker at room temperature unless indicated otherwise.

4G8 labeling was performed after pretreating brain sections with 70% formic acid (VWR<sup>®</sup>) for 20 min at room temperature. All tissues were then incubated in 30% hydrogen peroxide (Sigma-Aldrich<sup>®</sup>) diluted 1/100 for 20 min to inhibit endogenous peroxidases. Blocking of non-specific antigenic sites was achieved over 1 h using a 0.2% Triton X-100/0.1 M PBS (Sigma-Aldrich<sup>®</sup>) (PBST) solution containing 4.5% normal goat serum or 5% bovine serum albumin. Sections were then incubated at  $+4^{\circ}\text{C}$  with the 4G8 (Biolegend 800,706, 1/500) antibody diluted in a 3% NGS/PBST solution for 48 h. After rinsing, an incubation with the appropriate biotinylated secondary antibody diluted to 1/1000 in PBST was performed for 1 h at room temperature, followed by a 1 h incubation at room temperature with a 1:250 dilution of an avidin–biotin complex solution (ABC Vectastain kit, Vector Laboratories<sup>®</sup>). Revelation was performed using

the DAB Peroxidase Substrate Kit (DAB SK4100 kit, Vector Laboratories<sup>®</sup>). Sections were mounted on Superfrost Plus slides (Thermo-Scientific<sup>®</sup>). All sections were then dehydrated in successive baths of ethanol at  $50^{\circ}$ ,  $70^{\circ}$ ,  $96^{\circ}$  and  $100^{\circ}$  and in xylene. Slides were mounted with the Eukitt<sup>®</sup> mounting medium (Chem-Lab<sup>®</sup>).

Stained sections were scanned using an Axio Scan.Z1 (Zeiss<sup>®</sup>—Z-stack images acquired at  $20\times$  (z-stacks with 16 planes,  $1\ \mu\text{m}$  steps with extended depth of focus)). Each slice was extracted individually in the "czi" format using the Zen 2.0 (Zeiss<sup>®</sup>) software. Image processing and analysis were performed with the ImageJ 1.53i software. Macros were developed for each staining in order to attain a reproducible semi-automated quantification. Images were imported with a 50% reduction in resolution ( $0.44\ \mu\text{m}/\text{pixel}$ ), converted to the RGB format and saved as "tif". The 4G8 immunostaining was highlighted by color deconvolution with the H DAB vectors and by selecting the resulting DAB image. Then, segmentation was performed through an automatic local thresholding using the Phansalkar method (radius=50).  $\text{A}\beta$  load was evaluated after quantification of the 4G8-labeled particles between 7 and  $5,000\ \mu\text{m}^2$ , and normalization to the surface area of each region of interest (ROI).

All quantifications were performed on adjacent slices between 1.98 and  $-4.36$  mm from bregma. Eighteen adjacent slices were analyzed for the 4G8. All ROIs were manually segmented using ImageJ/FIJI, according to the Paxinos and Franklin neuro-anatomical atlas of mouse brain [33].

#### Evaluation of synaptic density

Synaptic density was evaluated in the hippocampus (CA1) and the perirhinal/entorhinal cortex of all inoculated mice using a double immunolabeling of presynaptic (Bassoon) and postsynaptic (Homer1) markers. Free-floating sections were permeabilized in a 0.5% Triton X-100/0.1 M PBS (Sigma-Aldrich<sup>®</sup>) solution for 15 min. Slices were incubated with Bassoon (Abcam Ab82958, 1/200) and Homer1 (Synaptic systems 160,003, 1/400) antibodies diluted in 3% BSA/PBST solution for 24 h at RT. Incubation with secondary antibodies coupled to a fluorochrome (Alexa Fluor) diluted in a 3% BSA/0.1 M PBS solution was then performed for 1 h at room temperature. Sections were rinsed and mounted on Superfrost Plus (Thermo-Scientific<sup>®</sup>) slides with the Vectashield<sup>®</sup> mounting medium with a refractive index of 1.45. Images of stained sections were acquired using a Leica DMI6000 confocal optical microscope (TCS SPE) with a  $40\times$  oil-immersion objective (refractive index 1.518) and the Leica Las X software. A confocal zoom of 3 and a pinhole aperture fixed at 1 Airy were applied.

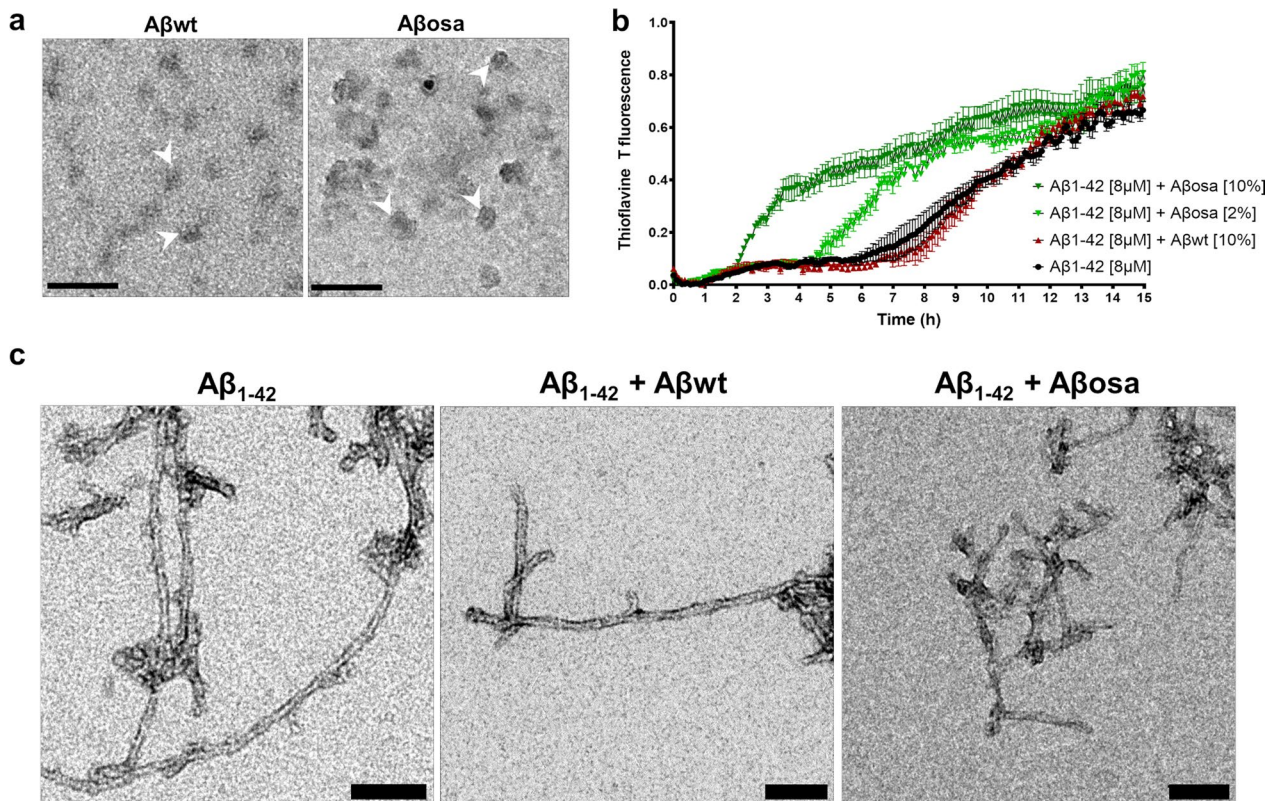


**Fig. 1** Properties of wt and mutated Aβ assemblies. **a.** Representative electron microscopy images of small and large particles in Aβ<sub>wt</sub> and Aβ<sub>osa</sub> solution. Scale bars: 100 nm. **b.** Kinetics of synthetic Aβ<sub>1-42</sub> aggregation monitored by thioflavin T fluorescence in the absence and presence of Aβ<sub>wt</sub> and Aβ<sub>osa</sub> seeds. Aggregation experiments were performed in triplicates. Aβ<sub>1-42</sub> monomer concentration is 8 μM, in a PBS buffer at 37 °C with continuous agitation. The aggregation curves were normalized to maximal values of ThT fluorescence at plateau. Symbols and error bars are the average and standard deviation, respectively, of three independent kinetics experiments. **c.** Representative electron microscopy images Aβ fibrils following the aggregation experiments. Scale bars: 100 nm

Acquisition was performed in sequential mode with a sampling rate of 1024 × 1024 and a scanning speed of 700 Hz. Image resolution was 80 nm/pixel and the optical section was 0.896 μm. 26 separate planes with a 0.2 μm step were acquired. The excitation wavelengths were 594 nm or 633 nm. Image acquisition in the dentate gyrus, CA1 and CA2/3 region was performed on 5 adjacent slices located between −1.58 and −3.40 mm from the bregma, with 3 images per slice. For the entorhinal cortex, 3 adjacent slices located between −2.98 and −3.40 mm from the bregma were analyzed, with 2 images acquired per slice. 3D deconvolution of the images was performed using the AutoQuant X3 software. The deconvoluted 8-bit images were analyzed using the ImageJ software, as described in Gilles et al. [13]. Briefly, automated 3D segmentation of the presynaptic (Bassoon) and postsynaptic (Homer1) stained deconvoluted images was performed using "3D spots segmentation" from ImageJ (with "gaussian fit", "block" and "no watershed" options; <https://imagej.net/plugins/3d-segmentation>). Co-localization of overlapping objects was evaluated

using "DiAna" from imageJ (<https://imagej.net/plugins/distance-analysis>). The percentage of colocalized objects was quantified as an index of synaptic density.

#### Statistical analysis

Statistical analysis was performed using the Graph-Pad Prism software 9. For the behavioral tasks analysis, Kruskal–Wallis tests with Dunn's multiple comparisons were performed except when repeated measures were acquired, in which case, a two-way repeated measures ANOVA with the Geisser-Greenhouse correction and Dunnett's multiple comparisons was carried out. For the post-mortem analysis, Kruskal–Wallis tests with Dunn's multiple comparisons tests were performed in order to compare differences between inoculated mice. The significance level was set at  $p < 0.05$ . Data are shown on scattered dot plots with mean ± standard error of the mean (SEM).



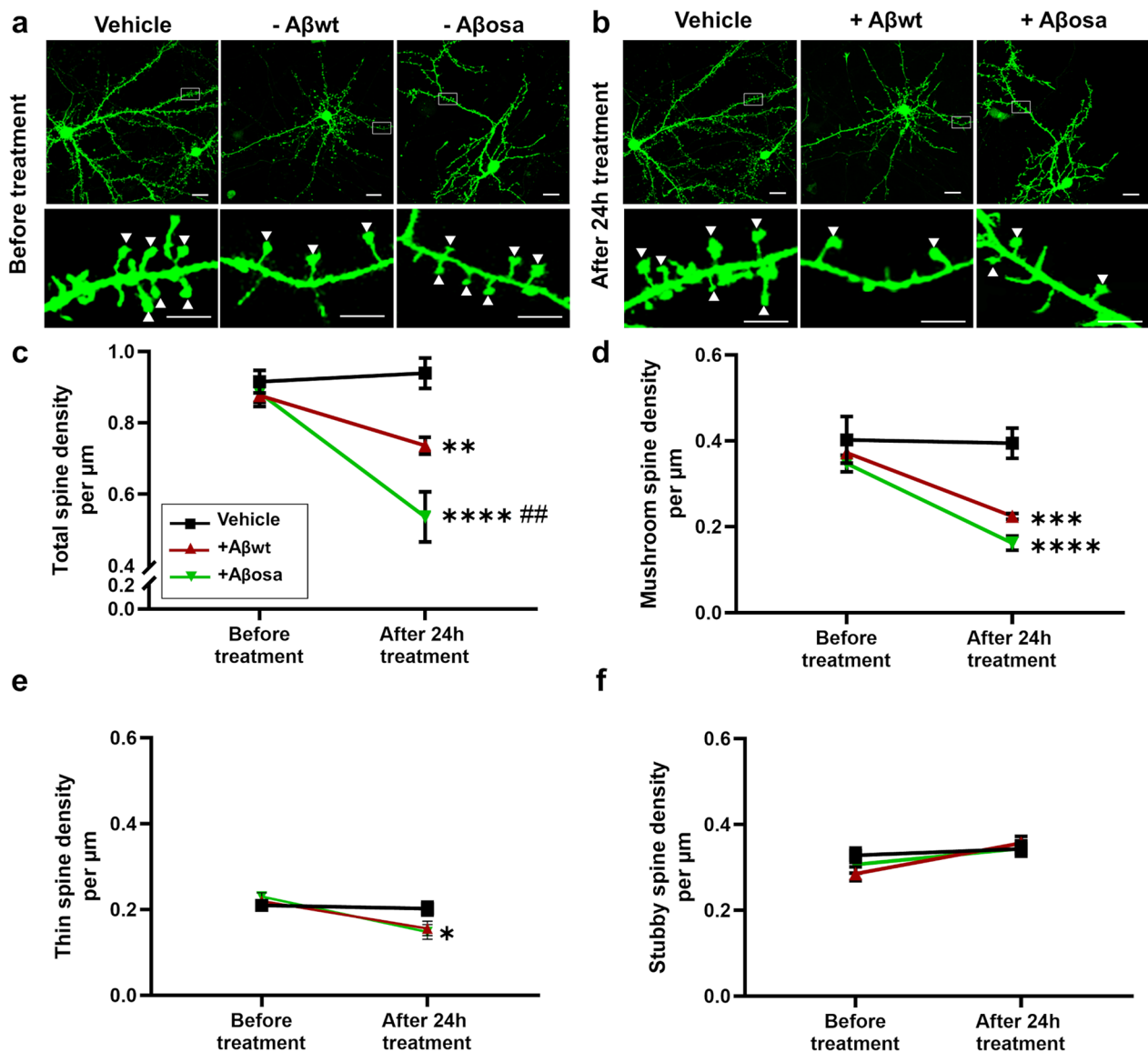


**Fig. 2** Exposure to exogenous Aβ<sub>osa</sub> and Aβ<sub>wt</sub> differentially impaired synapses. **a-b.** Representative images of primary cultures of cortical neurons expressing LA-GFP before (a), and after treatment for 24 h with 100 nM of Aβ<sub>osa</sub> or Aβ<sub>wt</sub> (b). Top row wide field view, scale bar = 10 μm; bottom row: dendrite portions with mushroom spines (white arrows, scale bar = 5 μm). **c.** Quantification of total spine density showed a reduction of total number of spines after treatment with Aβ<sub>osa</sub> and Aβ<sub>wt</sub>, compared to PBS (34.7 ± 3.1% for Aβ<sub>osa</sub>,  $p < 0.0001$ ; 14.1 ± 3.4% for Aβ<sub>wt</sub>,  $p = 0.0049$ ). The spine loss was significantly more severe in Aβ<sub>osa</sub> compared to Aβ<sub>wt</sub> ( $p = 0.0048$ ). **d.** Quantification of mushroom spine density showed a reduction of the number of mushroom spines after treatment with Aβ<sub>wt</sub> and Aβ<sub>osa</sub> (respectively  $p = 0.0005$  and  $p < 0.0001$ ). **e.** Quantification of thin spine density showed a reduction of the number of mushroom spines after treatment with Aβ<sub>osa</sub> ( $p < 0.1$ ). **f.** Stubby spine density was not modified after treatment with the different Aβ seeds.  $n = 6$  neurons from at least 3 different cultures. Data are shown as mean ± s.e.m. Kruskal–Wallis with Dunn’s multiple comparisons. \* $p < 0.05$ , \*\* or ##  $p < 0.05$ , \*\*\* $p < 0.005$ , \*\*\*\* $p < 0.0005$

#### Data availability

The data that support the findings of this study are available from the corresponding author, upon request.

#### Result

##### Characterization of inoculated Aβ peptides: from structures to synapse-modifying properties

We used a recombinant approach to produce non-mutated Aβ<sub>osa</sub> (E693Δ also called E22Δ) or Aβ<sub>1-42</sub> (Aβ<sub>wt</sub>). Electron micrographs showed that both Aβ peptides were able to self-aggregate and formed Aβ assemblies

in solutions (Fig. 1a). A $\beta$  aggregation is a nucleation-dependent polymerization process, with a slow initial nucleation phase, called lag-phase, followed by a rapid growth phase [18]. We investigated the seeding properties of different forms of A $\beta$  in vitro using thioflavin fluorescence assay [27, 32]. First, synthetic monomeric A $\beta_{1-42}$  was incubated at 37 °C, the ThT fluorescence signal displayed a sigmoidal shape characterized by a 6 h lag time followed by an 8 h elongation step (Fig. 1b). When synthetic monomeric A $\beta_{1-42}$  was seeded with recombinant A $\beta_{wt}$  [10%, v/v] at 37 °C, assembly kinetic was not affected while A $\beta$  fibrils were formed (Fig. 1b). On the contrary, addition of A $\beta_{osa}$  seeds [2 and 10%, v/v] shortened the lag time to 2 and 4 h respectively (Fig. 1b). Thus, A $\beta_{osa}$  displayed increased seeding effects. At steady state, the A $\beta$  fibrils assembled from synthetic A $\beta_{1-42}$  alone or seeded with A $\beta_{wt}$  or A $\beta_{osa}$  displayed undistinguishable shape when observed by electron microscopy (Fig. 1c).

### Exogenous application of A $\beta_{osa}$ and A $\beta_{wt}$ impairs synaptic plasticity and induces spine losses

As A $\beta$  has been shown to induce synaptic dysfunction [22], we compared the direct impact of A $\beta_{osa}$  and A $\beta_{wt}$  seeds on synaptic health by assessing spine morphology of primary cortical neuron cultures. Cortical neurons were co-transfected with LifeActin-GFP (LA-GFP), a small peptide that specifically binds to F-actin to visualize the dendritic arbor and spines. LA-GFP expressing cortical neurons display characteristic dendrites with a high density of spines (Fig. 2a). Then, we incubated the neurons with 100 nM of either A $\beta_{osa}$  or A $\beta_{wt}$  for 24 h, and analyzed thin, stubby, mushroom spine density (Fig. 2b-f). Compared to PBS, the total spine density of neurons treated with A $\beta_{osa}$  or A $\beta_{wt}$  was reduced at 24 h ( $p < 0.0001$  for A $\beta_{osa}$ ;  $p < 0.05$  for A $\beta_{wt}$ , Fig. 2c). The spine loss was significantly more severe in A $\beta_{osa}$  compared to A $\beta_{wt}$  ( $p < 0.05$ , Fig. 2c). The spine loss was mainly due to a strong reduction in mushroom ( $p < 0.0001$  for A $\beta_{osa}$ ;  $p < 0.005$  for A $\beta_{wt}$ , Fig. 2d) and thin spine densities ( $p < 0.5$

for A $\beta_{osa}$ , Fig. 2e) while stubby spine density was not significantly affected by A $\beta$  compared to PBS (Fig. 2f).

### A $\beta_{osa}$ inoculation to rodents impairs long-term memory

We then evaluated the long-term impact of A $\beta$  in vivo. Two-month-old APP<sub>swe</sub>/PS1<sub>de9</sub> mice were inoculated bilaterally with 0.5  $\mu$ g of A $\beta_{osa}$  or A $\beta_{wt}$  or PBS in the molecular layer of the dentate gyrus (MoDG) of the hippocampus. PBS was also inoculated in wild-type (WT) littermates. Behavioral assessment was performed at 4 months post-inoculation (mpi) using a novel object recognition task in a V-maze test (Fig. 3). First, the mice underwent a habituation to the test in an empty arena (day 1) followed by a training phase where two identical objects were added to the V-maze platform (day 2). Comparable interest in objects (Fig. 3a) and discrimination index (Fig. 3b) were observed during the training phase indicating similar exploratory activity between groups. The probe test (day 3) was performed the day following the training phase. During this task, a novel object replaced one of the objects. The traveled distance decreased throughout the three days of the test, but was comparable between groups (Fig. 3c). During the probe test, all groups of APP<sub>swe</sub>/PS1<sub>de9</sub> mice had comparable interest in objects (Fig. 3d). During the discrimination task, mice inoculated with A $\beta_{osa}$  spent less time exploring the novel object compared to control mice (PBS-inoculated WT or APP<sub>swe</sub>/PS1<sub>de9</sub> mice), suggesting memory impairments (Fig. 3e).

### A $\beta_{osa}$ inoculation leads to long-term functional impairments

To further evaluate brain function, we performed resting-state functional magnetic resonance imaging studies (fMRI) at 4 mpi. First, we analyzed the strength of the hippocampus functional connectivity (FC) to the whole-brain. The correlation coefficient between the hippocampus and other brain areas was lower in A $\beta_{osa}$ -inoculated animals compared to PBS and A $\beta_{wt}$ -inoculated mice (Fig. 4a). This indicates a decreased hippocampus

(See figure on next page.)

**Fig. 3** Memory impairment of APP<sub>swe</sub>/PS1<sub>de9</sub> mice following A $\beta$  inoculation. Novel object recognition was evaluated in a V-maze at 4 months post-inoculation. **a.** The time spent on exploring the two identical objects (in seconds) during the training phase is similar between group ( $p = 0.94$ ). **b.** Mice performance during the training phase. Similar discrimination indexes were found for all groups when mice had to discriminate two identical objects ( $p > 0.05$ , Kruskal–Wallis with Dunn's multiple comparisons). **c.** Distance moved throughout 3 days of tests (exploration, training and probe-test days). Measurements revealed a time-effect from day 1 to day 3 ( $F_{(1.49, 53.95)} = 123.8, p < 0.0005$ ), but no differences between experimental groups ( $p > 0.05$ ) (two-way repeated measures ANOVA with the Geisser-Greenhouse correction and Dunnett's multiple comparisons). **d.** Novel object recognition evaluated by the time spent on exploring the objects (in seconds) highlighted group effects ( $p = 0.02$ ). Post-hoc analysis showed that the PBS-inoculated wild-type mice group had a higher exploratory activity than PBS-inoculated APP<sub>swe</sub>/PS1<sub>de9</sub> ( $p = 0.02$ ) while all groups of APP<sub>swe</sub>/PS1<sub>de9</sub> mice had comparable exploratory activity (Kruskal–Wallis with Dunn's multiple comparisons). **e.** Object discrimination index. APP<sub>swe</sub>/PS1<sub>de9</sub> mice inoculated with A $\beta_{osa}$  spent less time exploring the novel object compared to PBS-inoculated WT mice or APP<sub>swe</sub>/PS1<sub>de9</sub> mice (group analysis using Kruskal–Wallis ( $p = 0.0006$ ) with post-hoc analysis using Dunn's multiple comparisons  $p = 0.0008$  and  $p = 0.0046$ , for A $\beta_{osa}$  versus PBS-inoculated WT and APP<sub>swe</sub>/PS1<sub>de9</sub> mice, respectively).  $n_{WT-PBS} = 10, n_{APP/PS1-PBS} = 10, n_{A\beta_{wt}} = 10, n_{A\beta_{osa}} = 10$  mice. Data are shown as mean  $\pm$  s.e.m

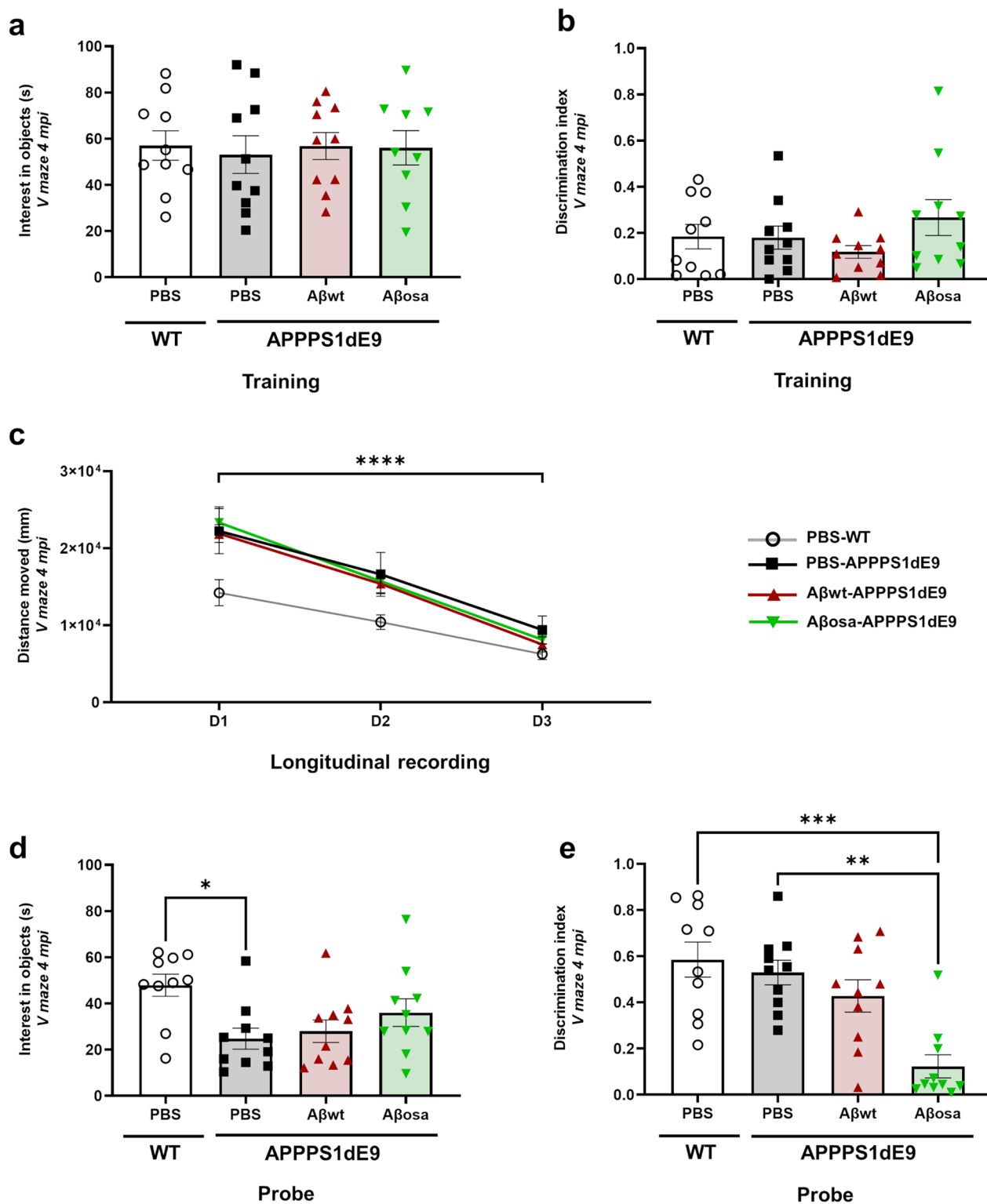


**Fig. 3** (See legend on previous page.)

connectivity in  $A\beta_{osa}$ -inoculated mice. To further identify specific networks impaired by  $A\beta_{osa}$  inoculation, we evaluated FC of three selected brain regions (right hemisphere) to the whole-brain: the MoDG (inoculation site), the CA1 area (which contains the pyramidal cell layer (CA $\pi$ ) and the entorhinal cortex (Fig. 4b). First we used a “seed-based analysis” (SBA), to identify regions functionally associated with each selected brain region in the PBS-inoculated APP<sub>swe</sub>/PS1<sub>DE9</sub> mice (Fig. 4c). The individual correlation maps were averaged for each group to highlight connected areas in each group of animals (Fig. 4d). Homotopic functional connectivity of MoDG was abolished in the contralateral dorsal dentate gyrus of  $A\beta_{osa}$ -inoculated mice while unaffected in  $A\beta_{wt}$ -inoculated animals (Fig. 4d). The MoDG and the CA1 of  $A\beta_{osa}$ -inoculated mice had also lower FC with the perihippocampal area, amygdalar area, temporal area and ventral CA1. The entorhinal cortex of  $A\beta_{osa}$ -inoculated mice had lower FC with the posterior cingulate, amygdala areas and the hippocampus area compared to PBS-inoculated mice (Fig. 4d). The alterations reported in  $A\beta_{osa}$  animals concerned both left-to-right (displayed figures) and right to left connectivities (not shown).

The individual correlation maps between groups were compared by performing voxel-wise statistical analysis. They confirmed differences between  $A\beta_{osa}$ - and PBS-inoculated APP<sub>swe</sub>/PS1<sub>DE9</sub> mice (Fig. 4e) and did not show differences between  $A\beta_{wt}$ - and PBS-inoculated mice (**not shown**). The FC alterations in  $A\beta_{osa}$ -inoculated animals that involve memory circuits are consistent with cognitive impairments reported in transgenic animals expressing  $A\beta_{osa}$  variant.

#### $A\beta_{osa}$ inoculation reduces synaptic density

Mice were sacrificed 4 mpi to evaluate cerebral pathology. We measured synaptic density at the inoculation site (dentate gyrus of the hippocampus), in other parts of the hippocampus and at a distant place (entorhinal cortex). Double immunolabeling of presynaptic (Bassoon) and postsynaptic (Homer) markers was performed

(Fig. 5a–b) and the amount of synapses was quantified from colocalized puncta. Inoculation of  $A\beta_{osa}$  led to decreased synaptic density in the dentate gyrus (Fig. 5c–e) and CA1 region (Fig. 5f–h) compared to APP<sub>swe</sub>/PS1<sub>DE9</sub> mice inoculated either with PBS or  $A\beta_{wt}$ . The decreased synaptic density was mainly related to a decrease in the density of postsynaptic markers as seen with Homer (Fig. 5e, h). Unlike  $A\beta_{osa}$ ,  $A\beta_{wt}$  did not modulate synaptic densities compared with PBS-inoculated animals (Fig. 5c–h). Synapses in the CA2/3 region and the entorhinal cortex were not affected by  $A\beta_{osa}$  or  $A\beta_{wt}$  (Fig. 5i–j). Taken together, these results indicate that a single inoculation of  $A\beta_{osa}$  has a long-term effect on synapse. Altogether our results suggest that inoculation of  $A\beta_{osa}$  increases a cascade of events leading to synaptic impairments, neuronal networks disorganization and cognitive impairments.

#### $A\beta_{osa}$ inoculation increases long-term A $\beta$ plaque deposition

Four mpi, A $\beta$  plaque load was increased at the inoculation site *i.e.* in the dentate gyrus of mice inoculated with  $A\beta_{osa}$  compared to APP<sub>swe</sub>/PS1<sub>DE9</sub> inoculated with PBS (Fig. 6a–c, 6j). Interestingly, A $\beta$  plaque load was also increased in regions connected to the inoculation site as the subiculum (Fig. 6l) and the entorhinal cortex (Fig. 6d–f, 5g), in animals inoculated with  $A\beta_{osa}$ . The A $\beta$  load was similar in the CA1 (**not shown**) and CA2/3 (**not shown**) of the three experimental groups. This can be explained by the low amyloid load in these regions. We did not find differences in plaque morphology (Fig. 6a–i). Taken together, these results indicate that inoculation of  $A\beta_{osa}$  increases A $\beta$  pathology at 4 mpi.

#### $A\beta_{osa}$ inoculation increases A $\beta$ oligomers and modulates APP processing

In order to evaluate if oligomer composition is affected by the inoculation of  $A\beta_{osa}$  in mice, we fractionated soluble and insoluble A $\beta$  aggregates from the hippocampus by sarkosyl detergent extraction. Western blot analysis of

(See figure on next page.)

**Fig. 4**  $A\beta_{osa}$  inoculated animals displayed abnormal brain connectivity within hippocampal-memory circuits. **a.** Mean hippocampus connectivity changes measured by resting-state functional MRI.  $A\beta_{osa}$ -inoculated group displayed a decreased hippocampus connectivity compared to PBS and  $A\beta_{wt}$ -inoculated mice at 4mpi (Kruskal–Wallis with Dunn’s multiple comparisons. group effect  $p=0.002$ ;  $p=0.006$  and  $p=0.01$  for  $A\beta_{osa}$ -inoculated group versus PBS or  $A\beta_{wt}$ -inoculated mice). **b.** 3D representation of the three brain regions –DG, CA1 and the entorhinal cortex– used for the seed-based analyses (SBA). **c.** SBA-derived resting state networks found in PBS-inoculated APP<sub>swe</sub>/PS1<sub>DE9</sub> are shown for each seed (the white asterisk represents the location of the seeds where the signal was extracted). **d.** Correlation maps of each seed. The color scale bar represents the strength of the functional correlation normalized with a fisher z-transformation. Black asterisks represent the location of the seeds. Differences are found between groups in inter-hemispheric homotopic FC. **e.** Voxelwise nonparametric permutation tests of FC correlation maps.  $A\beta_{osa}$ -inoculated mice have a lower FC in the hippocampus compared to PBS-inoculated mice ( $p < 0.001$ ). The color scale bar represents the statistical significant p-value. DG = dentate gyrus, Hipp = hippocampus, TE = temporal area, TEA = temporal associative area, Per/Ect = perirhinal + entorhinal cortex, Ins = Insular, Amg = amygdalar area, Ent = entorhinal cortex, PCC = posterior cingulate cortex, SSC = primary somatosensory area, Str = striatum.  $n_{WT-PBS} = 10$ ,  $n_{APP/PS1-PBS} = 10$ ,  $n_{A\beta_{wt}} = 10$ ,  $n_{A\beta_{osa}} = 10$  mice

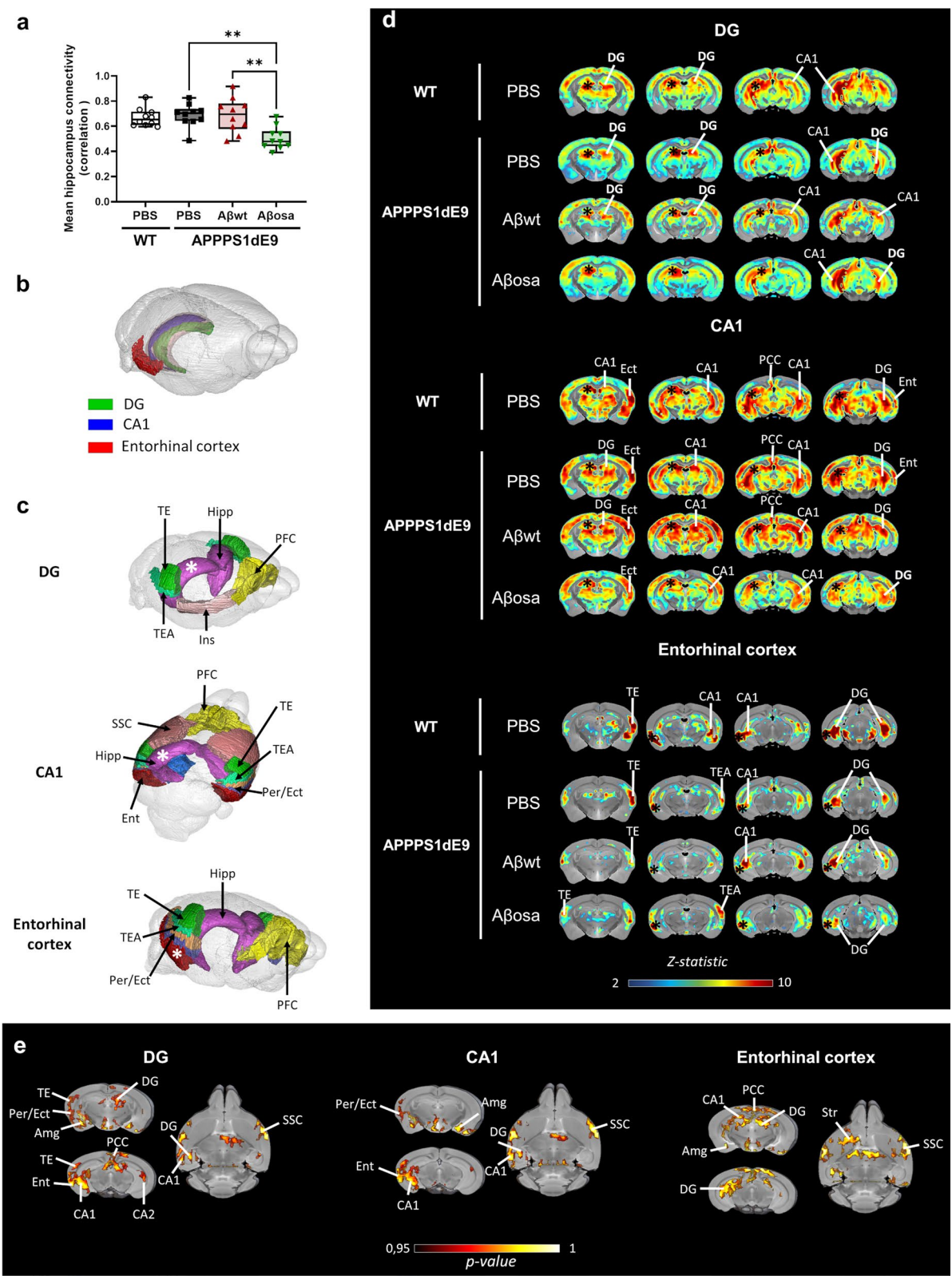


**Fig. 4** (See legend on previous page.)

sarkosyl-soluble fraction showed an increase of 15 kDa and 12kDa bands (also referred as 4-mer and 3-mer forms of A $\beta$  oligomers [28]) in A $\beta_{\text{osa}}$ -inoculated animals (Fig. 7a). On the contrary, A $\beta_{\text{wt}}$  did not affect amyloid oligomer profiles as compared to PBS. The enrichment in multimeric/assembled forms of A $\beta$  was confirmed by dot blot analysis using conformational antibodies against oligomers (A11) and fibrils (OC). We observed that both species increased in the hippocampus of A $\beta_{\text{osa}}$ -inoculated APP<sub>swe</sub>/PS1<sub>dE9</sub> mice compared to WT mice (Fig. 7b–d). Taken together, these results support the hypothesis that A $\beta$  seeds are able to modulate A $\beta$  aggregation processes up to 4 mpi.

An alternative hypothesis is that A $\beta_{\text{osa}}$  modulated APP processing [36]. To test this hypothesis, we assessed APP proteolytic profiles caused by  $\alpha$ - or  $\beta$ -secretase pathways in the hippocampus at 4 mpi. We quantified by Western blot  $\alpha$ -CTF (C83, 9kDa) and  $\beta$ -CTF (C99, 11 kDa) (Fig. 7e–f). We found an increase of  $\alpha$ -CTF and  $\beta$ -CTF following A $\beta_{\text{osa}}$  inoculation compared to PBS and A $\beta_{\text{wt}}$ -inoculation in APP<sub>swe</sub>/PS1<sub>dE9</sub> mice, suggesting that A $\beta_{\text{osa}}$  seeds modulate APP processing in vivo (Fig. 7e–f).

## Discussion

We showed that intracerebral inoculation of A $\beta_{\text{osa}}$  seeds in the hippocampus of a mouse model of amyloidosis worsens the clinical outcome associated with A $\beta$  deposition 4 mpi. This leads to cognitive and synaptic impairments, reduced functional connectivity between brain regions involved in memory circuits, increased focal A $\beta$  plaque deposition at the inoculation site and spreading of A $\beta$  in the brain as well as increased presence of A $\beta$  oligomers and modulation of APP processing.

### Amyloid deposition and spreading induced by A $\beta_{\text{osa}}$

The A $\beta$  deposition induced by A $\beta_{\text{osa}}$  inoculation in APP<sub>swe</sub>/PS1<sub>dE9</sub> transgenic mice can be interpreted using mechanistic models explaining prion diseases. They

suggest that in presence of preformed amyloid seeds, newly produced non- $\beta$ -sheet monomers can change their conformation to assemble into novel aggregated amyloid structures thus inducing a self-propagating process [18]. APP<sub>swe</sub>/PS1<sub>dE9</sub> transgenic mice express human-like A $\beta_{1-40}$  and A $\beta_{1-42}$  peptides [16] and do not express A $\beta_{\text{osa}}$ . Thus, likely, A $\beta_{\text{osa}}$  increased aggregation of endogenous A $\beta_{1-40}$  or A $\beta_{1-42}$  peptides. Our Thioflavin binding aggregation assay showing that A $\beta_{\text{osa}}$  has pro-aggregative properties in presence of A $\beta_{1-42}$  is consistent with this hypothesis. Several studies have shown that inoculum containing A $\beta$  are eliminated from the brain on the days following the inoculation [19, 52]. It is thus reasonable to assume that A $\beta_{\text{osa}}$  seeds were eliminated from the brains on the days following their inoculation. The long-term effects of the single inoculation of A $\beta_{\text{osa}}$  can thus be explained by an early increase of A $\beta$  deposition induced by A $\beta_{\text{osa}}$ . As we detected changes of APP processing, another non-exclusive hypothesis is that, following A $\beta_{\text{osa}}$  inoculation and subsequent increased A $\beta$  deposition, APP processing was shifted towards increased A $\beta$  production as shown in [36]. This hypothesis however still has to be validated in vivo.

It is interesting to outline that A $\beta_{\text{osa}}$  inoculation not only modulated quantitatively the amyloid plaque load, but also increased A $\beta$  oligomers. In addition to a local effect in the dentate gyrus, inoculation of A $\beta_{\text{osa}}$  induced increased A $\beta$  deposition in the entorhinal cortex, *i.e.* at distance of the inoculation site. The spreading of A $\beta$  from the inoculum site to interconnected brain regions has already been reported in mice and this has been interpreted as related to a self-propagating process [7, 53]. In our study, it is likely that, the spreading seeds were secondary A $\beta$  seeds produced locally at the inoculation site by the host after A $\beta_{\text{osa}}$  inoculation. We can however not rule out that A $\beta_{\text{osa}}$  seeds spread in the entorhinal cortex just after its inoculation to induce A $\beta$  aggregation in this region.

(See figure on next page.)

**Fig. 5** A $\beta_{\text{osa}}$  exacerbates long-term synaptotoxicity in vivo. **a.** Representative views of original Bassoon/Homer images and segmented puncta in APP<sub>swe</sub>/PS1<sub>dE9</sub> mice. Scale bars main images: 20  $\mu\text{m}$ ; Insets: 5  $\mu\text{m}$ . **b.** Co-localisation puncta of Bassoon/Homer labels (white arrow). Scale bars main images: 5  $\mu\text{m}$ ; Insets: 1  $\mu\text{m}$ . **c–h.** Quantification of synaptic density from Bassoon/Homer colocalization (**c, f**), Bassoon (**d, g**) and Homer (**e, h**) in the dentate gyrus and CA1 showed decrease of synaptic density and post-synaptic density (Homer) in the dentate gyrus and CA1 of A $\beta_{\text{osa}}$ -inoculated APP<sub>swe</sub>/PS1<sub>dE9</sub> mice (**c**): Bassoon/Homer in dentate gyrus—overall effect:  $p < 0.0001$  (Kruskal–Wallis). Post-hoc evaluation with Dunn's multiple comparisons: A $\beta_{\text{osa}}$ - versus PBS-inoculated APP<sub>swe</sub>/PS1<sub>dE9</sub>:  $p < 0.0001$ ; A $\beta_{\text{wt}}$ - versus A $\beta_{\text{osa}}$ -inoculated APP<sub>swe</sub>/PS1<sub>dE9</sub>:  $p = 0.003$ ; **e**: Homer in dentate gyrus—overall effect:  $p = 0.0015$  (Kruskal–Wallis). Post-hoc evaluation with Dunn's multiple comparisons: A $\beta_{\text{osa}}$ - versus PBS-inoculated APP<sub>swe</sub>/PS1<sub>dE9</sub>:  $p = 0.0029$ ; A $\beta_{\text{wt}}$ - versus A $\beta_{\text{osa}}$ -inoculated APP<sub>swe</sub>/PS1<sub>dE9</sub>:  $p = 0.0058$ ; **f**: Bassoon/Homer in CA1—overall effect:  $p = 0.002$  (Kruskal–Wallis). Post-hoc evaluation with Dunn's multiple comparisons: A $\beta_{\text{osa}}$ - versus PBS-inoculated animals:  $p = 0.002$ ; **h**: Homer in CA1—overall effect:  $p = 0.0535$  (Kruskal–Wallis). Post-hoc evaluation with Dunn's multiple comparisons: A $\beta_{\text{osa}}$ - versus PBS-inoculated APP<sub>swe</sub>/PS1<sub>dE9</sub>:  $p = 0.0469$ . There were no changes in the different groups in the CA2/3 (**i**) and in the entorhinal cortex (**j**).  $n_{\text{APP/PS1-PBS}} = 10$ ,  $n_{\text{A}\beta_{\text{wt}}} = 10$ ,  $n_{\text{A}\beta_{\text{osa}}} = 10$  mice. For each image, quantification was made on 26 sections separated by 0.2  $\mu\text{m}$  step. A surface of  $81.92 * 81.92 \mu\text{m}^2$  was measured for each section. Data are shown as mean  $\pm$  s.e.m

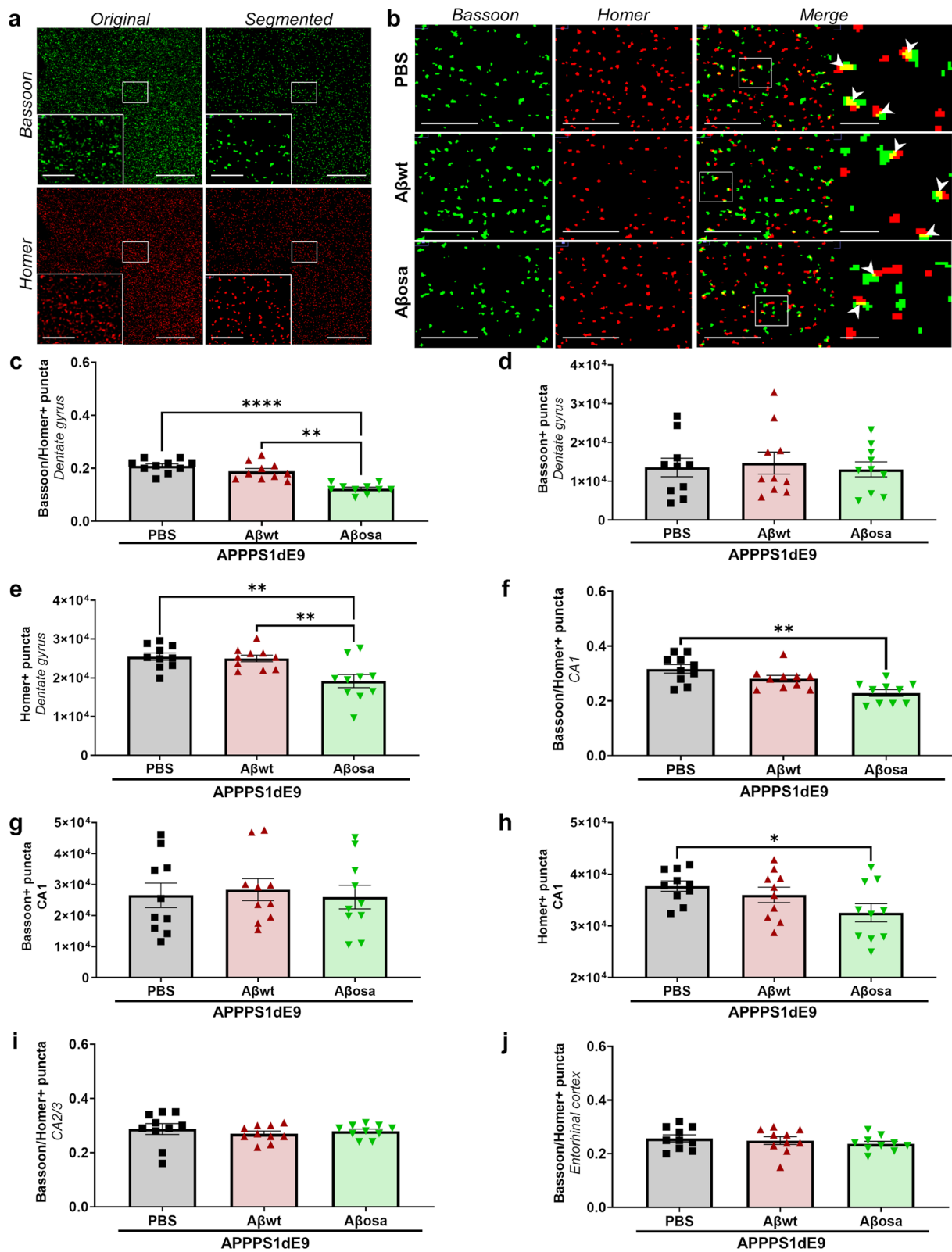


**Fig. 5** (See legend on previous page.)

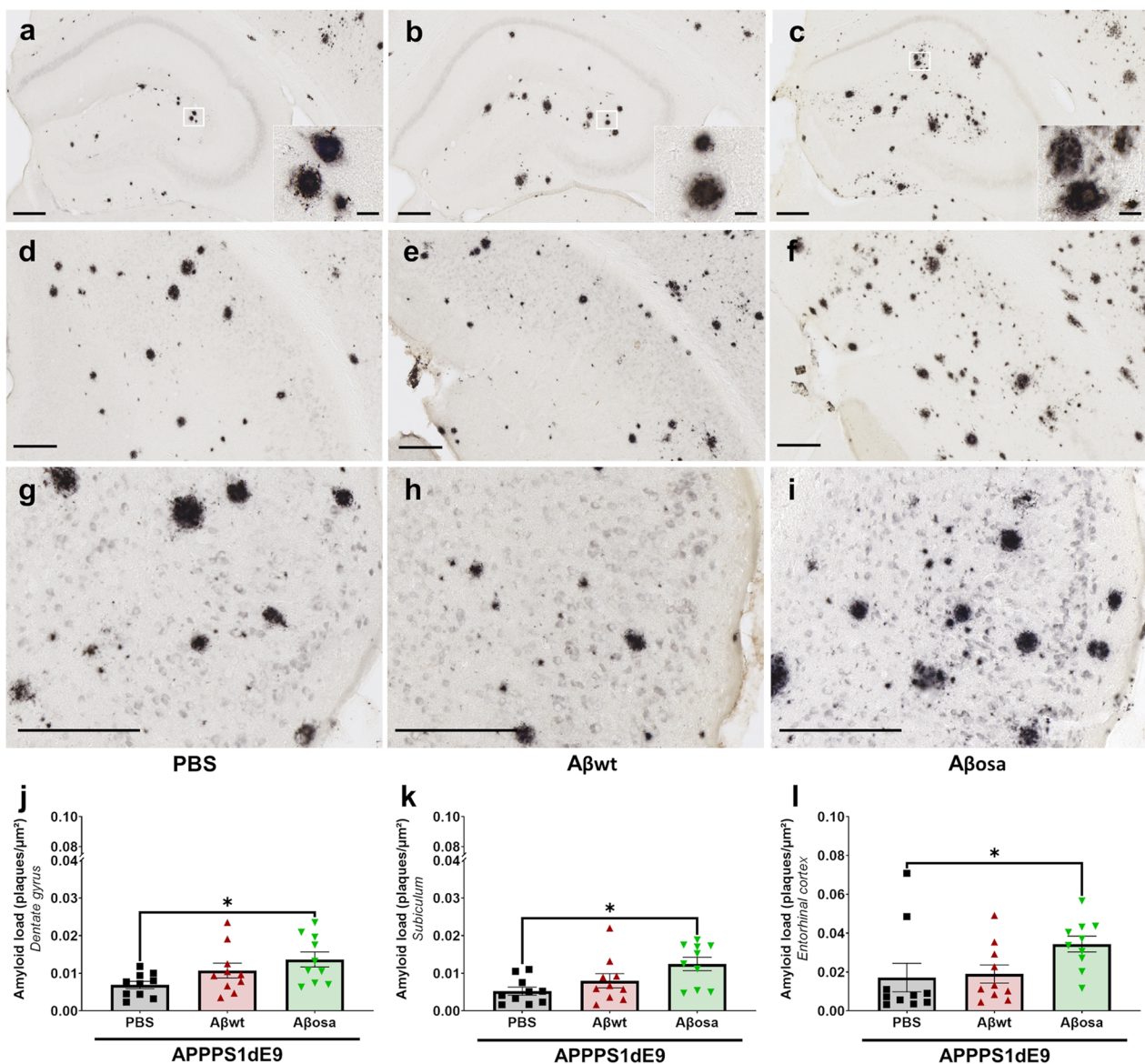


**Fig. 6** Modulation of A $\beta$  plaque load following inoculation of A $\beta$  variants. Representative images of 4G8 immunolabeling showing A $\beta$  plaque deposition in the dorsal hippocampus (a–c), subiculum (d–f) and entorhinal cortex (g–i) of APP<sub>swe</sub>/PS1<sub>dE9</sub> mice after PBS, A $\beta$ <sub>wt</sub> or A $\beta$ <sub>osa</sub> inoculation in the dentate gyrus. **j–l**. Quantification of amyloid load (4G8-positive amyloid plaques per  $\mu\text{m}^2$ ) in the dentate gyrus (j), in the subiculum (k), and in the entorhinal cortex (l). A $\beta$ <sub>osa</sub> increases A $\beta$  plaque deposition in the dentate gyrus ( $p = 0.04$ ), in the subiculum ( $p = 0.02$ ), in the entorhinal cortex ( $p = 0.02$ ). Kruskal–Wallis with Dunn’s multiple comparisons.  $n_{\text{APP/PS1-PBS}} = 10$ ,  $n_{\text{A}\beta\text{wt}} = 10$ ,  $n_{\text{A}\beta\text{osa}} = 10$  mice. Data are shown as mean  $\pm$  s.e.m. Scale bars main images: 200  $\mu\text{m}$ ; Insets: 20  $\mu\text{m}$

### Long-term pathological cascades following A $\beta$ <sub>osa</sub> inoculation

We found that the cascade of events induced by A $\beta$ <sub>osa</sub> is able to induce cognitive and synaptic impairments 4 mpi. To our knowledge, long-term effects of synthetic or recombinant A $\beta$  seeds on cognition or synaptic impairments had not been reported. As A $\beta$  is known to induce

synaptic deficits either ex vivo or in transgenic mouse models [38, 40, 41], it is reasonable to consider that the increased A $\beta$  plaque deposition and A $\beta$  oligomers induced by A $\beta$ <sub>osa</sub> was, at least in part, responsible for the cognitive and synaptic impairments detected in A $\beta$ <sub>osa</sub>-inoculated APP<sub>swe</sub>/PS1<sub>dE9</sub> mice. Local A $\beta$  plaque deposition may however not be the sole culprit in synaptic



impairments as A $\beta$  was not changes in the CA1 after A $\beta_{\text{osa}}$ -inoculation while synaptic density was reduced. Soluble forms of amyloid could be the culprit. Alternatively, the synaptic impairments could be the consequence of A $\beta$ -related neuronal impairments in projecting neurons. Interestingly, we showed that A $\beta$ -associated pathology induced by A $\beta_{\text{osa}}$  occurred locally and was generalized to the entorhinal cortex. We also found that inoculation of A $\beta_{\text{osa}}$  affects both local hippocampus functional connectivity and global connections within networks. This contributes to the assumption of an AD-like disconnection syndrome in the inoculated mice. This global disconnection occurs mainly in brain areas connected to the hippocampus and the entorhinal cortex in which A $\beta$  deposits accumulated. Although A $\beta$  build-up seems to trigger the pathological cascade, primary effect linked to A $\beta_{\text{osa}}$  it-self cannot be excluded. Notably, the interplay between accumulation of A $\beta_{\text{osa}}$  aggregates and synaptic or memory impairments have been hinted by others in several in vitro and ex vivo studies [21, 45–47].

#### Differences between a single A $\beta_{\text{osa}}$ inoculation in transgenic mice and pathologies developed by patients or mice producing A $\beta_{\text{osa}}$

Extracellular A $\beta$  plaques are rare in patients with A $\beta_{\text{osa}}$  mutations or in transgenic mice expressing human APP695 with the Osaka mutation (APP<sub>E693 $\Delta$</sub> -Tg mice). These mice express the mutation under the mouse prion protein promoter and have a C57BL/6 background [45]. They have an APP expression level similar to those of endogenous mouse APP and they do not show any A $\beta$  plaques even at 24 months but display an age-dependent accumulation of A $\beta$  oligomers within neurons [29, 45]. Our results showing increased A $\beta$  depositions observed in mice following A $\beta_{\text{osa}}$  inoculation was unexpected given the lack of A $\beta$  plaques in humans and APP<sub>E693 $\Delta$</sub> -Tg mice. Thus, A $\beta_{\text{osa}}$  triggers different processes when it is secreted at physiological level and when it is used as an exogenous seed in mice overexpressing A $\beta_{1-40}$  or A $\beta_{1-42}$ .

#### Limitations of the study

In our study, we chose to study the impact of A $\beta_{\text{osa}}$  inoculation in 6-month-old APP<sub>swe</sub>/PS1<sub>dE9</sub> mice, *i.e.* 4 mpi. In these mice, in the absence of any inoculum, A $\beta$  is continuously secreted and the first A $\beta$  plaques occur in 4-month-old animals, while in 6 month-old animals, they have reached the cortex and the hippocampus. In a previous study, we showed that, in these mice, A $\beta$  plaque load is increased at the inoculation site 4 months after intrahippocampal Alzheimer human brain extract inoculation [24]. Our result with A $\beta_{\text{osa}}$  is consistent with this result, but showed a spreading of A $\beta$  plaques and cognitive alterations that were not detected at 4 mpi after human brain extract inoculation. Thus, the pathology induced by A $\beta_{\text{osa}}$  seems more severe than that induced by Alzheimer brain extracts. Unexpectedly, at 4 mpi, A $\beta_{\text{wt}}$  inoculation had no effect on A $\beta$  plaque deposition. The A $\beta_{\text{wt}}$  that we used displayed typical characteristics of A $\beta$ , *i.e.* self-aggregating and synaptotoxic properties in vitro. It is possible that pro-aggregation properties of our recombinant A $\beta_{\text{wt}}$  was lower than that of A $\beta_{\text{osa}}$  or human Alzheimer extracts. Thus, animal models that show A $\beta$  deposition more slowly are required to dissociate spontaneous and induced deposition induced by A $\beta_{\text{wt}}$ . Consistently with this suggestion, the induction of A $\beta$  plaques by synthetic A $\beta_{1-42}$  (corresponding to A $\beta_{\text{wt}}$ ) seeds has been reported in mice only after 11 or 13 months post-inoculation in slowly evolving models [43, 44]. A complementary hypothesis is that recombinant A $\beta_{1-42}$  was less toxic than synthetic A $\beta_{1-42}$ . To our knowledge, recombinant A $\beta_{1-42}$  seeds have never been used for experimental transmission of A $\beta$  in vivo and it is difficult to extrapolate results from synthetic to recombinant seeds as they display different aggregation properties [9, 50].

(See figure on next page.)

**Fig. 7** APP proteolysis profiles and oligomerization of amyloid- $\beta$  peptides at 4 mpi. **a.** Western-blot analysis (6E10 Antibody) of total human APP and A $\beta$  oligomeric species in sarkosyl-soluble extracts of the hippocampus of APP<sub>swe</sub>/PS1<sub>dE9</sub> mice after PBS, A $\beta_{\text{wt}}$  or A $\beta_{\text{osa}}$  inoculation at 4mpi. Full length APP runs at an apparent molecular size of 110 kDa, oligomeric forms of A $\beta$  are detected at 15 kDa and 12 kDa. **b.** Dot blot analysis for oligomeric species (A11) and fibrils (OC) in sarkosyl-soluble extract from the hippocampus. **c.** Quantification of relative expression levels of A11 are presented. A $\beta_{\text{osa}}$  increased oligomer forms compared to PBS- ( $p = 0.0019$ ), A $\beta_{\text{wt}}$ -inoculated ( $p = 0.0106$ ) APP<sub>swe</sub>/PS1<sub>dE9</sub> and WT mice ( $p = 0.0142$ ). **d.** Quantification of relative expression levels of OC are presented. A $\beta_{\text{osa}}$  increased fibrils compared to A $\beta_{\text{wt}}$ -inoculated ( $p = 0.0038$ ) APP<sub>swe</sub>/PS1<sub>dE9</sub> and WT mice ( $p = 0.0118$ ). **e.** Western-blot analysis (APP-Cter-17 antibody) of total endogenous APP, APP-CTFs and tubulin in hippocampus lysates (S100K fractions) obtained from wild-type and APP<sub>swe</sub>/PS1<sub>dE9</sub> mice after PBS, A $\beta_{\text{wt}}$  or A $\beta_{\text{osa}}$  inoculation. Tubulin staining was used as a marker and loading control. **f-g.** Semi-quantification of APP (APP-Cter-C17 Antibody (**f**)) and of  $\beta$ -CTF/C99 and  $\alpha$ -CTF/C83 (APP-Cter-C17 Antibody (**g**)) [39]. Kruskal–Wallis with Dunn's multiple comparisons. \* $p < 0.5$ , \*\* $p < 0.05$ , \*\*\* $p < 0.005$ , \*\*\*\* $p < 0.0005$ . nWT<sub>PBS</sub> = 2, nAPP/PS1<sub>PBS</sub> = 4, nA $\beta_{\text{wt}}$  = 4, nA $\beta_{\text{osa}}$  = 4 mice. Data are shown as mean  $\pm$  s.e.m

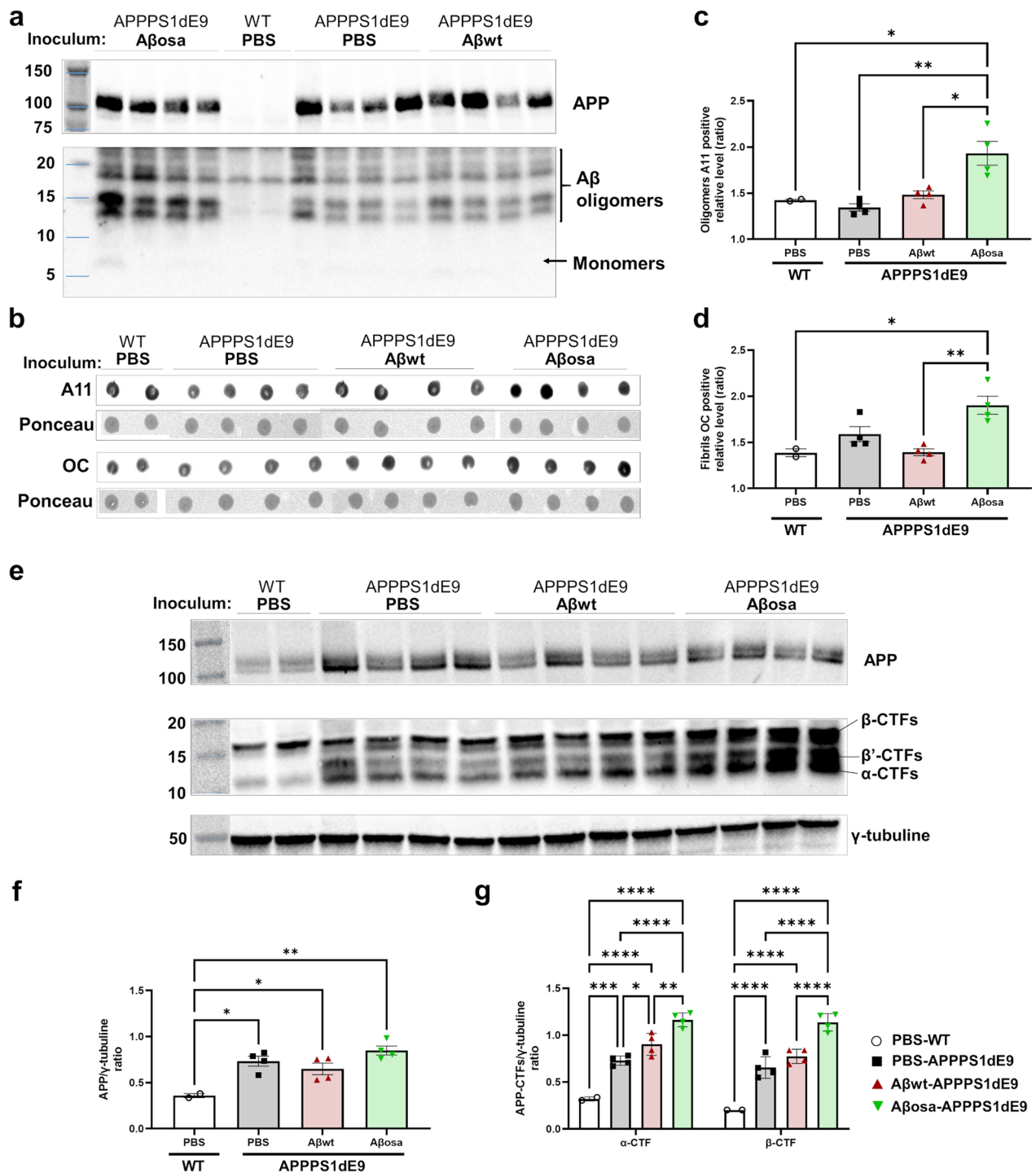


**Fig. 7** (See legend on previous page.)

### Conclusion

We showed that a single inoculation of A $\beta$ <sub>osa</sub> induces a long-term cascade of events leading to increased A $\beta$  aggregation and A $\beta$  oligomers in the brain. These events

impair synaptic health, leading to cerebral network reorganization and cognitive impairments. This is the first study showing long-term functional toxicity of A $\beta$  seeds. These results suggest that a single, sporadic event as

$A\beta_{\text{osa}}$  inoculation can worsen the fate of the pathology and clinical outcome several months after the event. Further studies are now required to evaluate links between the structure of  $A\beta_{\text{osa}}$  and its toxic effects.

#### Abbreviations

A $\beta$	Amyloid- $\beta$
AD	Alzheimer's disease
Mpi	Months post-inoculation
APP	Amyloid precursor protein
PS1	Presenilin 1
WT	Wild-type
ThT	Thioflavin T
SBA	Seed-based analysis

#### Acknowledgements

We thank Martine Guillermier and Mylène Gaudin for surgical expertise during inoculation of proteins to animals. We thank Nicolas Heck for his help in synapse quantification. This work has benefited from the platform and expertise of the Electron Microscopy Facility of I2BC. We thank Nicolas Sergeant for providing the APP-Cter-17 antibody.

#### Author contributions

MC, ASH, AB, and MD. contributed to the study conception and design. MJS, EB, AB provided the recombinant  $A\beta$  proteins. MC performed the inoculations in mice. MC designed and performed memory evaluations, MC, JBP, MD designed and performed connectivity studies, MC, ASH, FP, designed and performed the immunohistological analysis in animals. MC, MJS, and AB performed biochemical analysis. MC, LB performed Thioflavin aggregation assays and electron microscopy. MJS, EB, AB performed ex vivo experiments on cell cultures. MC, AB, and MD wrote the manuscript. All authors commented on previous versions of the manuscript. All authors read and approved the final manuscript.

#### Funding

The project was funded by the Fondation Vaincre Alzheimer 2018 and the Association France-Alzheimer 2021. It was performed in a core facility supported by/member of NeurATRIS—ANR-11-INBS-0011. It was also supported by internal funds from the Laboratory of Neurodegenerative Diseases and MIRcen. MC was financed by the French Ministère de l'Enseignement Supérieur, de la Recherche, et de l'Innovation. The funding sources had no role in the design of the study, in the collection, analysis, and interpretation of data, nor in writing the manuscript.

#### Availability of data and materials

The data that support the findings of this study are available from the corresponding author.

#### Declarations

##### Ethics approval and consent to participate

All experimental procedures were conducted in accordance with the European Community Council Directive 2010/63/UE and approved by local ethics committees (CEtEA-CEA DSV IdF N°44, France) and the French Ministry of Education and Research, and in compliance with the 3R guidelines. Animal care was supervised by a dedicated veterinarian and animal technicians.

##### Consent for publication

Does not apply to the content of this article.

##### Competing interests

The authors declare that they have no competing interests.

##### Author details

<sup>1</sup>Laboratoire Des Maladies Neurodégénératives, Université Paris-Saclay, CEA, CNRS, 18 Route du Panorama, 92265 Fontenay-Aux-Roses, France. <sup>2</sup>Commissariat À L'Énergie Atomique Et Aux Énergies Alternatives (CEA), Direction de La

Recherche Fondamentale (DRF), Institut François Jacob, MIRcen, 18 Route du Panorama, 92265 Fontenay-aux-Roses, France. <sup>3</sup>Univ. Grenoble Alpes, Inserm, U1216, Grenoble Institut Neurosciences, GIN, 38000 Grenoble, France.

Received: 17 February 2023 Accepted: 25 March 2023

Published online: 22 April 2023

#### References

1. Abraham A, Pedregosa F, Eickenberg M, Gervais P, Mueller A, Kossaifi J, Gramfort A, Thirion B, Varoquaux G (2014) Machine learning for neuroimaging with scikit-learn. *Front Neuroinform*. <https://doi.org/10.3389/fninf.2014.00014>
2. Balducci C, Beeg M, Stravalaci M, Bastone A, Sclip A, Biasini E, Tapella L, Colombo L, Manzoni C, Borsello T, Chiesa R, Gobbi M, Salmons M, Forloni G (2010) Synthetic amyloid-beta oligomers impair long-term memory independently of cellular prion protein. *Proc Natl Acad Sci USA* 107:2295–2300. <https://doi.org/10.1073/pnas.0911829107>
3. Célestine M, Nadkarni NA, Garin C, Bougacha S, Dhenain M (2020) Samba-MRI, a library for small animal neuroimaging data processing in Python. *Front Neuroinform*. <https://doi.org/10.3389/fninf.2020.00024>
4. Dorr AE, Lerch JP, Spring S, Kabani N, Henkelman RM (2008) High resolution three-dimensional brain atlas using an average magnetic resonance image of 40 adult C57Bl/6J mice. *Neuroimage* 42:60–69. <https://doi.org/10.1016/j.neuroimage.2008.03.037>
5. du Sert NP, Hurst V, Ahluwalia A, Alam S, Avey MT, Baker M, Browne WJ, Clark A, Cuthill IC, Dirnagl U, Emerson M, Garner P, Holgate ST, Howells DW, Karp NA, Lázic SE, Lidster K, MacCallum CJ, Macleod M, Pearl EJ, Petersen OH, Rawle F, Reynolds P, Rooney K, Sena ES, Silberberg SD, Steckler T, Wurbel H (2020) The ARRIVE guidelines 20: Updated guidelines for reporting animal research. *Bmc Veterinary Research*. <https://doi.org/10.1186/s12917-020-02451-y>
6. Duyckaerts C, Sazdovitch V, Ando K, Seilhean D, Privat N, Yilmaz Z, Peckeu L, Amar E, Comoy E, Maceski A, Lehmann S, Brion JP, Brandel JP, Haik S (2018) Neuropathology of iatrogenic Creutzfeldt-Jakob disease and immunoassay of French cadaver-sourced growth hormone batches suggest possible transmission of tauopathy and long incubation periods for the transmission of Abeta pathology. *Acta Neuropathol* 135:201–212. <https://doi.org/10.1007/s00401-017-1791-x>
7. Eisele YS, Bolmont T, Heikenwalder M, Langer F, Jacobson LH, Yan ZX, Roth K, Aguzzi A, Staufenbiel M, Walker LC, Jucker M (2009) Induction of cerebral beta-amyloidosis: intracerebral versus systemic Abeta inoculation. *Proc Natl Acad Sci USA* 106:12926–12931. <https://doi.org/10.1073/pnas.0903200106>
8. Epelbaum S, Youssef I, Lacor PN, Chaurand P, Duplus E, Brugg B, Duyckaerts C, Delatour B (2015) Acute amnesic encephalopathy in amyloid-beta oligomer-injected mice is due to their widespread diffusion in vivo. *Neurobiol Aging* 36:2043–2052. <https://doi.org/10.1016/j.neurobiolaging.2015.03.005>
9. Finder VH, Vodopivec I, Nitsch RM, Glockshuber R (2010) The recombinant amyloid-beta peptide A beta 1–42 aggregates faster and is more Neurotoxic than Synthetic A beta 1–42. *J Mol Biol* 396:9–18. <https://doi.org/10.1016/j.jmb.2009.12.016>
10. Friston KJ, Holmes AP, Worsley KJ, Poline JP, Frith CD, Frackowiak RSJ (1994) Statistical parametric maps in functional imaging: a general linear approach. *Hum Brain Mapp* 2:189–210. <https://doi.org/10.1002/hbm.460020402>
11. Garcia-Alloza M, Robbins EM, Zhang-Nunes SX, Purcell SM, Betensky RA, Raju S, Prada C, Greenberg SM, Bacskaï BJ, Frosch MP (2006) Characterization of amyloid deposition in the APP<sup>swE</sup>/PS1<sup>dE9</sup> mouse model of Alzheimer disease. *Neurobiol Dis* 24:516–524. <https://doi.org/10.1016/j.nbd.2006.08.017>
12. Gary C, Lam S, Herard AS, Koch JE, Petit F, Gipchtein P, Sawiak SJ, Caillierez R, Eddarkaoui S, Colin M, Aujard F, Deslys JP, Network FN, Brouillet E, Buée L, Comoy EE, Pifferi F, Picq J-L, Dhenain M (2019) Encephalopathy induced by Alzheimer brain inoculation in a non-human primate. *Acta Neuropathol Commun* 7:126. <https://doi.org/10.1186/s40478-019-0771-x>
13. Gilles JF, Dos Santos M, Boudier T, Bolte S, Heck N (2017) DiAna, an ImageJ tool for object-based 3D co-localization and distance analysis. *Methods* 115:55–64. <https://doi.org/10.1016/j.jmeth.2016.11.016>

14. Herve D, Porche M, Cabrejo L, Guidoux C, Tournier-Lasserre E, Nicolas G, Adle-Biassette H, Plu I, Chabriat H, Duyckaerts C (2018) Fatal Abeta cerebral amyloid angiopathy 4 decades after a dural graft at the age of 2 years. *Acta Neuropathol* 135:801–803. <https://doi.org/10.1007/s00401-018-1828-9>
15. Jang H, Arce FT, Ramachandran S, Kagan BL, Lal R, Nussinov R (2014) Disordered amyloidogenic peptides may insert into the membrane and assemble into common cyclic structural motifs. *Chem Soc Rev* 43:6750–6764. <https://doi.org/10.1039/c3cs60459d>
16. Jankowsky JL, Fadale DJ, Anderson J, Xu GM, Gonzales V, Jenkins NA, Copeland NG, Lee MK, Younkin LH, Wagner SL, Younkin SG, Borchelt DR (2004) Mutant presenilins specifically elevate the levels of the 42 residue beta-amyloid peptide in vivo: evidence for augmentation of a 42-specific gamma secretase. *Hum Mol Genet* 13:159–170. <https://doi.org/10.1093/hmg/ddh019>
17. Jaunmuktane Z, Mead S, Ellis M, Wadsworth JD, Nicoll AJ, Kenny J, Launchbury F, Linehan J, Richard-Loendt A, Walker AS, Rudge P, Collinge J, Brandner S (2015) Evidence for human transmission of amyloid-beta pathology and cerebral amyloid angiopathy. *Nature* 525:247–250. <https://doi.org/10.1038/nature15369>
18. Jucker M, Walker LC (2013) Self-propagation of pathogenic protein aggregates in neurodegenerative diseases. *Nature* 501:45–51. <https://doi.org/10.1038/nature12481>
19. Kane MD, Lipinski WJ, Callahan MJ, Bian F, Durham RA, Schwarz RD, Roher AE, Walker LC (2000) Evidence for seeding of beta-amyloid by intracerebral infusion of Alzheimer brain extracts in beta-amyloid precursor protein-transgenic mice. *J Neurosci* 20:3606–3611. <https://doi.org/10.1523/JNEUROSCI.20-10-03606.2000>
20. Koffie RM, Hyman BT, Spires-Jones TL (2011) Alzheimer's disease: synapses gone cold. *Mol Neurodegrad*. <https://doi.org/10.1186/1750-1326-6-63>
21. Kulic L, McAfoose J, Welt T, Tackenberg C, Spani C, Wirth F, FINDER V, Konietzko U, Giese M, Eckert A, Noriaki K, Shimizu T, Murakami K, Irie K, Rasool S, Glabe C, Hock C, Nitsch RM (2012) Early accumulation of intracellular fibrillar oligomers and late congophilic amyloid angiopathy in mice expressing the Osaka intra-A beta APP mutation. *Translational Psychiatry*. <https://doi.org/10.1038/tp.2012.109>
22. Lacor PN, Buniel MC, Chang L, Fernandez SJ, Gong Y, Viola KL, Lambert MP, Velasco PT, Bigio EH, Finch CE, Krafft GA, Klein WL (2004) Synaptic targeting by Alzheimer's-related amyloid beta oligomers. *J Neurosci* 24:10191–10200. <https://doi.org/10.1523/JNEUROSCI.3432-04.2004>
23. Laemmli UK (1970) Cleavage of structural proteins during assembly of head of bacteriophage-T4. *Nature*. <https://doi.org/10.1038/227680a0>
24. Lam S, Herard AS, Boluda S, Petit F, Eddarkaoui S, Cambon K, Picq JL, Buee L, Duyckaerts C, Haik S, Dhenain M (2022) Pathological changes induced by Alzheimer's brain inoculation in amyloid-beta plaque-bearing mice. *Acta Neuropathol Commun* 10:112. <https://doi.org/10.1186/s40478-022-01410-y>
25. Lam S, Petit F, Hérad A-S, Boluda S, Eddarkaoui S, Guillermier M, Network T-C, Buee L, Duyckaerts C, Haik S, Picq J-L, Dhenain M (2021) Transmission of amyloid-beta and tau pathologies is associated with cognitive impairments in a primate. *Acta Neuropathol Commun* 9:165. <https://doi.org/10.1186/s40478-021-01266-8>
26. Leveille F, El Gaamouch F, Goux E, Lecocq M, Lobner D, Nicole O, Buisson A (2008) Neuronal viability is controlled by a functional relation between synaptic and extrasynaptic NMDA receptors. *Faseb J* 22:4258–4271. <https://doi.org/10.1096/fj.08-107268>
27. LeVine H (1999) Quantification of beta-sheet amyloid fibril structures with thioflavin T. *Amyloid, Prions, and Other Protein Aggregates* 309:274–284. [https://doi.org/10.1016/S0076-6879\(99\)09020-5](https://doi.org/10.1016/S0076-6879(99)09020-5)
28. Lutzenberger M, Burwinkel M, Riemer C, Bode V, Baier M (2015) Ablation of CCAAT/enhancer-binding protein delta (C/EBPD): Increased plaque burden in a murine Alzheimer's disease model. *Plos One* 10:e0134228. <https://doi.org/10.1371/journal.pone.0134228>
29. Matsuyama S, Teraoka R, Mori H, Tomiyama T (2007) Inverse correlation between amyloid precursor protein and synaptic plasticity in transgenic mice. *Neuroreport* 18:1083–1087. <https://doi.org/10.1097/Wnr.0b013e3281e72b18>
30. Meyer-Luehmann M, Coomaraswamy J, Bolmont T, Kaeser S, Schaefer C, Kilger E, Neuenschwander A, Abramowski D, Frey P, Jaton AL, Vigouret JM, Paganetti P, Walsh DM, Mathews PM, Ghiso J, Staufenbiel M, Walker LC, Jucker M (2006) Exogenous induction of cerebral beta-amyloidogenesis is governed by agent and host. *Science* 313:1781–1784. <https://doi.org/10.1126/science.1131864>
31. Novotny R, Langer F, Mahler J, Skodras A, Vlachos A, Wegenast-Braun BM, Kaeser SA, Neher JJ, Eisele YS, Pietrowski MJ, Nilsson KPR, Deller T, Staufenbiel M, Heimrich B, Jucker M (2016) Conversion of synthetic a beta to in vivo active seeds and amyloid plaque formation in a hippocampal slice culture model. *J Neurosci* 36:5084–5093. <https://doi.org/10.1523/Jneurosci.0258-16.2016>
32. Ono K, Takahashi R, Ikeda T, Mizuguchi M, Hamaguchi T, Yamada M (2014) Exogenous amyloidogenic proteins function as seeds in amyloid beta-protein aggregation. *Biochim Biophys Acta* 1842:646–653. <https://doi.org/10.1016/j.bbadis.2014.01.002>
33. Paxinos G, Franklin KBJ (2001) The mouse brain in stereotaxic coordinates. Academic Press, City
34. Richards K, Watson C, Buckley RF, Kurniawan ND, Yang ZY, Keller MD, Beare R, Bartlett PF, Egan GF, Galloway GJ, Paxinos G, Petrou S, Reutens DC (2011) Segmentation of the mouse hippocampal formation in magnetic resonance images. *Neuroimage* 58:732–740. <https://doi.org/10.1016/j.neuroimage.2011.06.025>
35. Rodriguez A, Ehlenberger DB, Dickstein DL, Hof PR, Wearne SL (2008) Automated three-dimensional detection and shape classification of dendritic spines from fluorescence microscopy images. *Plos One* 3:e1997. <https://doi.org/10.1371/journal.pone.0001997>
36. Rolland M, Powell R, Jacquier-Sarlin M, Boisseau S, Reynaud-Dulaurier R, Martinez-Hernandez J, André L, Borel E, Buisson A, Lanté F (2020) Interaction of Aβ oligomers with neuronal APP triggers a vicious cycle leading to the propagation of synaptic plasticity alterations to healthy neurons. *J Neurosci* 40:5161–5176. <https://doi.org/10.1523/Jneurosci.2501-19.2020>
37. Schutz AK, Vagt T, Huber M, Ovchinnikova OY, Cadalbert R, Wall J, Guntert P, Bockmann A, Glockshuber R, Meier BH (2015) Atomic-resolution three-dimensional structure of amyloid beta fibrils bearing the Osaka mutation. *Angewandte Chemie-Int Edition* 54:331–335. <https://doi.org/10.1002/anie.201408598>
38. Selkoe DJ (2002) Alzheimer's disease is a synaptic failure. *Science* 298:789–791. <https://doi.org/10.1126/science.1074069>
39. Sergeant N, David JP, Champain D, Ghestem A, Watzet A, Delacourte A (2002) Progressive decrease of amyloid precursor protein carboxy terminal fragments (APP-CTFs), associated with tau pathology stages, in Alzheimer's disease. *J Neurochem* 81:663–672. <https://doi.org/10.1046/j.1471-4159.2002.00901.x>
40. Sivanesan S, Tan A, Rajadas J (2013) Pathogenesis of abeta oligomers in synaptic failure. *Curr Alzh Res* 10:316–323. <https://doi.org/10.2174/1567205011310030011>
41. Spires-Jones TL, Hyman BT (2014) The intersection of amyloid beta and tau at synapses in Alzheimer's disease. *Neuron* 82:756–771. <https://doi.org/10.1016/j.neuron.2014.05.004>
42. Steadman PE, Ellegood J, Szulc KU, Turnbull DH, Joyner AL, Henkelman RM, Lerch JP (2014) Genetic effects on cerebellar structure across mouse models of autism using a magnetic resonance imaging atlas. *Autism Res* 7:124–137. <https://doi.org/10.1002/aur.1344>
43. Stohr J, Condello C, Watts JC, Bloch L, Oehler A, Nick M, DeArmond SJ, Giles K, DeGrado WF, Prusiner SB (2014) Distinct synthetic Abeta prion strains producing different amyloid deposits in bigenic mice. *Proc Natl Acad Sci USA* 111:10329–10334. <https://doi.org/10.1073/pnas.1408968111>
44. Stohr J, Watts JC, Mensinger ZL, Oehler A, Grillo SK, Dearmond SJ, Prusiner SB, Giles K (2012) Purified and synthetic Alzheimer's amyloid beta (Abeta) prions. *Proc Natl Acad Sci USA* 109:11025–11030. <https://doi.org/10.1073/pnas.1206555109>
45. Tomiyama T, Matsuyama S, Iso H, Umeda T, Takuma H, Ohnishi K, Ishibashi K, Teraoka R, Sakama N, Yamashita T, Nishitsuji K, Ito K, Shimada H, Lambert MP, Klein WL, Mori H (2010) A mouse model of amyloid beta oligomers: Their contribution to synaptic alteration, abnormal tau phosphorylation, glial activation, and neuronal loss in vivo. *J Neurosci* 30:4845–4856. <https://doi.org/10.1523/Jneurosci.5825-09.2010>
46. Tomiyama T, Nagata T, Shimada H, Teraoka R, Fukushima A, Kanemitsu H, Takuma H, Kuwano R, Imagawa M, Ataka S, Wada Y, Yoshioka E, Nishizaki T, Watanabe Y, Mori H (2008) A new amyloid beta variant favoring oligomerization in Alzheimer's-type dementia. *Ann Neurol* 63:377–387. <https://doi.org/10.1002/ana.21321>

47. Tomiyama T, Shimada H (2020) APP Osaka mutation in familial Alzheimer's disease—its discovery, phenotypes, and mechanism of recessive inheritance. *Int J Mol Sci* 21:1413. <https://doi.org/10.3390/ijms21041413>
48. Ullmann JFP, Watson C, Janke AL, Kurniawan ND, Reutens DC (2013) A segmentation protocol and MRI atlas of the C57BL/6J mouse neocortex. *Neuroimage* 78:196–203. <https://doi.org/10.1016/j.neuroimage.2013.04.008>
49. Ulm BS, Borchelt DR, Moore BD (2021) Remodeling Alzheimer-amyloidosis models by seeding. *Mol Neurodegener* 16:8. <https://doi.org/10.1186/s13024-021-00429-4>
50. Varshavskaya KB, Mitkevich VA, Makarov AA, Barykin EP (2022) Synthetic, cell-derived, brain-derived, and recombinant beta-amyloid: modelling Alzheimer's Disease for research and drug development. *Int J Mol Sci* 23:15036. <https://doi.org/10.3390/ijms232315036>
51. Vingtdeux V, Hamdane M, Gompel M, Begard S, Drobecq H, Ghestem A, Grosjean ME, Kostanjevecki V, Grognet P, Vanmechelen E, Buee L, Delacourte A, Sergeant N (2005) Phosphorylation of amyloid precursor carboxy-terminal fragments enhances their processing by a gamma-secretase-dependent mechanism. *Neurobiol Dis* 20:625–637. <https://doi.org/10.1016/j.nbd.2005.05.004>
52. Ye L, Fritschy SK, Schelle J, Obermuller U, Degenhardt K, Kaeser SA, Eisele YS, Walker LC, Baumann F, Staufenbiel M, Jucker M (2015) Persistence of Abeta seeds in APP null mouse brain. *Nat Neurosci* 18:1559–1561. <https://doi.org/10.1038/nn.4117>
53. Ye L, Hamaguchi T, Fritschy SK, Eisele YS, Obermuller U, Jucker M, Walker LC (2015) Progression of seed-induced Abeta deposition within the limbic connectome. *Brain Pathol* 25:743–752. <https://doi.org/10.1111/bpa.12252>

## Publisher's Note

Springer Nature remains neutral with regard to jurisdictional claims in published maps and institutional affiliations.

Ready to submit your research? Choose BMC and benefit from:

- fast, convenient online submission
- thorough peer review by experienced researchers in your field
- rapid publication on acceptance
- support for research data, including large and complex data types
- gold Open Access which fosters wider collaboration and increased citations
- maximum visibility for your research: over 100M website views per year

At BMC, research is always in progress.

Learn more [biomedcentral.com/submissions](https://biomedcentral.com/submissions)

